Key Emerging Issues and Recent Progress related to Structural Materials Degradation (PWRs, VVERs and CANDUs)

Author

François Cattant
Plescop, France

A.N.T. INTERNATIONAL®

Advanced Nuclear Technology International
Analysvägen 5, SE-435 33 Mölnlycke
Sweden

info@antinternational.com
www.antinternational.com

Ecolabelled printed matter, 3041 0129

Disclaimer

The information presented in this report has been compiled and analysed by Advanced Nuclear Technology International Europe AB (ANT International®) and its subcontractors. ANT International has exercised due diligence in this work, but does not warrant the accuracy or completeness of the information. ANT International does not assume any responsibility for any consequences as a result of the use of the information for any party, except a warranty for reasonable technical skill, which is limited to the amount paid for this assignment by each LCC programme member.

Contents

1 A few words about the "Fontevraud" conference.

The first "Fontevraud" conference was held in 1985. A first objective of this conference was to highlight the failure root cause analysis work performed by French laboratories, especially the EDF ones. A second goal was to allow Utilities to exchange information regarding field failures and plant maintenance.

The operating and maintenance experiences targeted by the "Fontevraud" conference are those resulting from materials failure or degradation.

From 1985 ("Fontevraud I") to 2006 ("Fontevraud VI"), the conference took place in the Royal Abbey of Fontevraud, one of the largest monastic cities in the western Christendom, right in the heart of the Loire Valley. Even if the conference moved to Avignon in 2010 ("Fontevraud VII") and was also held in the Popes' Palace in 2014 ("Fontevraud VIII"), the original name of the symposium was kept, due to its unique program.

Originally, "Fontevraud" was only PWRs but in 2006, the scope of the conference was extended to BWRs too. This same year, a track dedicated to civil engineering was added to the program.

165 papers were presented at "Fontevraud VIII", in September 2014, with the following breakdown:

- 108 papers dedicated to PWRs materials issues;
- 17 papers dedicated to BWRs materials issues;
- 17 papers applying to both PWRs and BWRs;
- 23 papers in the "civil engineering" track,

Here only the 108 papers dedicated to PWRs (including VVERs and CANDUs) materials issues along with 11 papers applying to both PWRs and BWRs are going to be reported, the other 46 papers are reported separately.

These 119 papers are sorted into 9 tracks:

- Pressure vessel;
- Pressure vessel internals;
- Stainless steels corrosion;
- Nickel alloys corrosion;
- Piping, pump and valves;
- Steam generator;
- Steam-water systems;
- Turbine and alternator;
- Fuel and control rod assembly.

2 Discussion & conclusion

2.1 General comments

This document has two main sections.

The first section contains brief descriptions (average of 5 to 10 lines) of each of the 119 papers in order to give the reader an overview of the content of the original papers.

The second section contains extended summaries (in general 2 to 3 pages) of all the papers.

The two sections have the same organization: same chapters/sections titles and same order of appearance for the papers.

The main characteristics of this 2014 Fontevraud conference are:

There are more papers dedicated to Alloy 690 than to Alloy 600. Part of this is due to the fact that more and more A600 components are replaced with A690 components. But another reason is that the factor of improvement stemming from switching from 15% Cr alloys to 30% Cr alloys is not yet well established and thus more research is required to refine this factor.

Another observation is that LTCP seems to be of less concern for researcher's community. Same thing with zinc injection: zinc injection is now common and thus doesn't require extensive research anymore, although some laboratories still have programs dedicated to zinc injection issues.

On another hand, because of the extension of 30% Cr alloys use, more and more research programs are launched on LRO understanding and risk.

It is worth mentioning that there is more and more reporting of examples of component's failures in an oxidizing environment although occurring in a PWR. There are more and more examples coming out from the literature, partly because of the implementation of news sophisticated tools, which are tuned to detect cracking in an oxidizing environment. For example Renate Kilian has presented the cracking of baffle bolts from German PWRs which occurred under oxidizing environment [Kilian et al, 2014].

One very good news for all PWR utilities is that the IGSCC of the stainless steel SG safe end of Mihama 2 should be arrested or had negligible small CGR before detection and this IGSCC should be specific matter, not generic matter in PWR.

2.2 Pressure vessel

2.2.1 Classical surveillance program

To take full benefit of the pressure vessel track presentations, it is necessary to know how the classical surveillance program or RPV steel under irradiation is set up. The reference [Chaouadi & Gérard, 2014] presents a good summary of a classical surveillance program.

It must be recalled that for historical reasons related to the post-World War II state-of-the-art scientific knowledge and pragmatic engineering solutions, the Charpy impact test is the reference test used to evaluate the degradation of RPV materials, including base metal, weld and heat affected zone. In particular, the key property that is used for RPV integrity assessment is the ductile-to-brittle transition temperature. The procedures that were developed within the ASME code are essentially empirical and rely on a number of correlations. One of these correlations is the indexation of the lower bound fracture toughness curve through a single variable, the reference temperature of nil ductility transition. By knowing only this single material property, the RT_{NDT}, the static and dynamic lower bound fracture toughness curves necessary for structural integrity assessments can be determined.

The RT_{NDT} determination is based on a combination of drop weight tests to determine the temperature of nil ductility transition and Charpy impact tests for the DBTT. The drop weight test, often referred to as 'Pellini' test, was developed at the Naval Research Laboratory, Washington DC, as a simple method to determine the nil-ductility transition temperature. The NDTT was defined in the 1950s [Puzak et al, 1952] as the test temperature in explosion bulge tests at which the plate remained flat at fracture, that is crack propagation occurred in the presence of elastic strains only. The drop-weight test was developed to simplify the determination of the NDTT, it is standardised in ASTM E208.

Typical drop-weight equipment is illustrated in Figure 2-1 and test specimen in Figure 2-2. It consists of a rectangular coupon with a brittle weld bead deposited on one face. The weld contains a notch, from which a crack is initiated by impact loading the specimen to a fixed amount of deformation under three-point bend (Figure 2-3). Tests are carried out at a variety of temperatures, the NDTT being defined as the maximum temperature at which the brittle crack spreads completely across one or both of the tension surfaces on either side of the brittle weld bead.

Figure 2-1: Typical Pellini drop weight test equipment (www.wance.net).

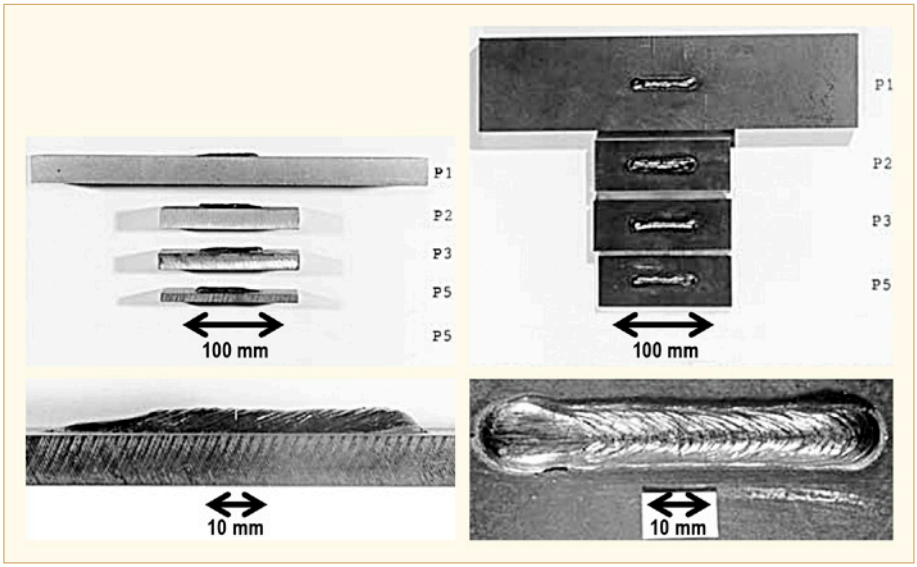

Figure 2-2: Drop-weight test specimens. Left: side view, the lower photo shows close-up of weld-bead and notch. Right: top view of the specimens, the lower photo shows close-up of weld-bead with central notch just visible as thin black line [TWI, 2015].

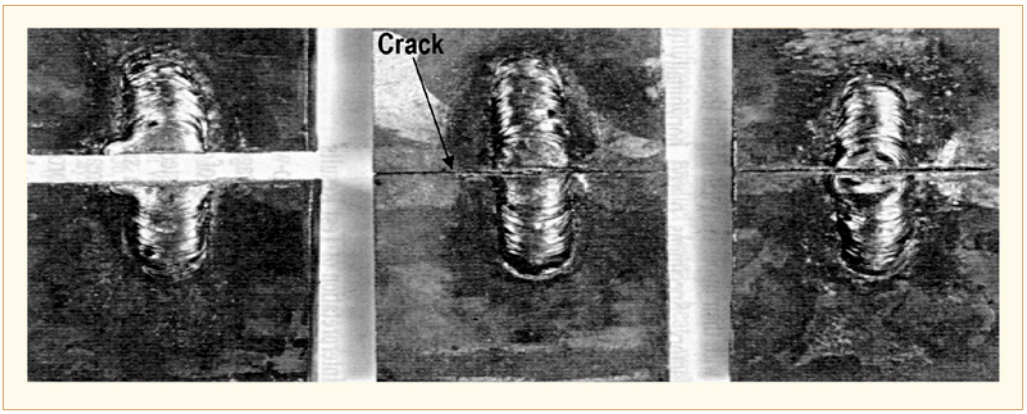

Figure 2-3: View of cracked Pellini specimens.

The importance of the NDTT as a reference temperature for the ductile to brittle transition temperature of ferritic steels was established from studies of service failures and structurally representative crack arrest tests. The correlation between the structural fracture transition behaviour and NDTT was originally established for 1940s ship steels; however, it was subsequently found that the NDTT could also be applied to reference the fracture transition of fully killed and alloy steels as well as quench and tempered steels. Given its importance as a fracture transition reference temperature, correlations between the NDTT and structurally representative test results continue to be sought.

The NDT temperature is determined by Pellini drop-weight tests in accordance with ASTM E-208. If the minimum impact energy and lateral expansion of 3 Charpy-V tests performed at NDT +33°C are at least 68 J and 0.89 mm respectively, the NDT temperature is taken to represent the RT_{NDT}. If the Charpy-V properties do not meet the above criterion, RT_{NDT} is taken 33°C below the temperature at which these requirements are reached. In most cases, however, the RT_{NDT} is governed by the Pellini NDT.

There are also requirements on the upper shelf energy, which should be at least equal to 102 J before irradiation. After irradiation, it should exceed at any time 68 J.

The ASME lower bound for static fracture toughness, K_{IC}, is given by:

Eq. 2-1: $$K_{Ic} = 36.48 + 22.78 \cdot \exp[0.036\ (T - RT_{NDT})]$$

Under dynamic loading, the ASME lower bound fracture toughness, K_{Id}, is the reference lower bound, K_{IR}, given by:

Eq. 2-2: $$K_{IR} = K_{Id} = 29.45 + 13.68 \cdot \exp[0.026\ (T - RT_{NDT})]$$

These two ASME curves are enveloping all available fracture toughness data obtained on large fracture toughness test specimens. The static K_{Ic} ASME lower bound fracture toughness curve is used in accidental conditions while the dynamic K_{IR} ASME lower bound fracture toughness curve is used in normal operation conditions.

The diagram depicted in Figure 2-4 shows how the ASME lower bound fracture toughness in the irradiated condition is determined according to the prevailing regulatory rules. In the unirradiated condition, the RT_{NDT} is determined using both Pellini drop weight tests and Charpy impact tests. Once this temperature is determined, it can be used in the ASME lower bound fracture toughness equation.

Upon irradiation, it is assumed that the RT_{NDT} shift is equal to the T_{41J}-shift. By using Charpy impact tests in the unirradiated and irradiated conditions, the transition curves can be determined according to the following fitting hyperbolic tangent equation:

Eq. 2-3: $$E(T) = \frac{E_{USE} + E_{LSE}}{2} + \frac{E_{USE} - E_{LSE}}{2} \cdot \tanh\left(\frac{T - T_{transition}}{T_{slope}}\right)$$

where E is the absorbed energy, E_{USE} is the upper shelf energy plateau, E_{LSE} is the lower shelf energy plateau usually taken equal to 0, $T_{transition}$ is the transition temperature and T_{slope} is the slope of the transition curve. By fitting the experimental data, namely absorbed energy versus test temperature data points, the following four parameters can be determined, E_{USE} , E_{LSE} (=0), $T_{transition}$ and T_{slope}. The transition curve is then fully determined using Eq. 2-3. The same expression as Eq. 2-3 can be used for the shear fracture appearance and lateral expansion.

The T_{41J} can then be derived as:

Eq. 2-4: $$T_{41J} = T_{transition} + T_{slope} \times a\tanh\left(\frac{2 \times 41 - E_{USE} - E_{LSE}}{E_{USE} - E_{LSE}}\right)$$

The RT_{NDT} of the irradiated material can then easily be derived using:

Eq. 2-5: $$RT_{NDT}^{irrad} = RT_{NDT}^{unirrad} + \Delta T_{41J}$$

Subsequently, the corresponding ASME lower bound fracture toughness curve can easily be derived for the irradiated condition (see Figure 2-4).

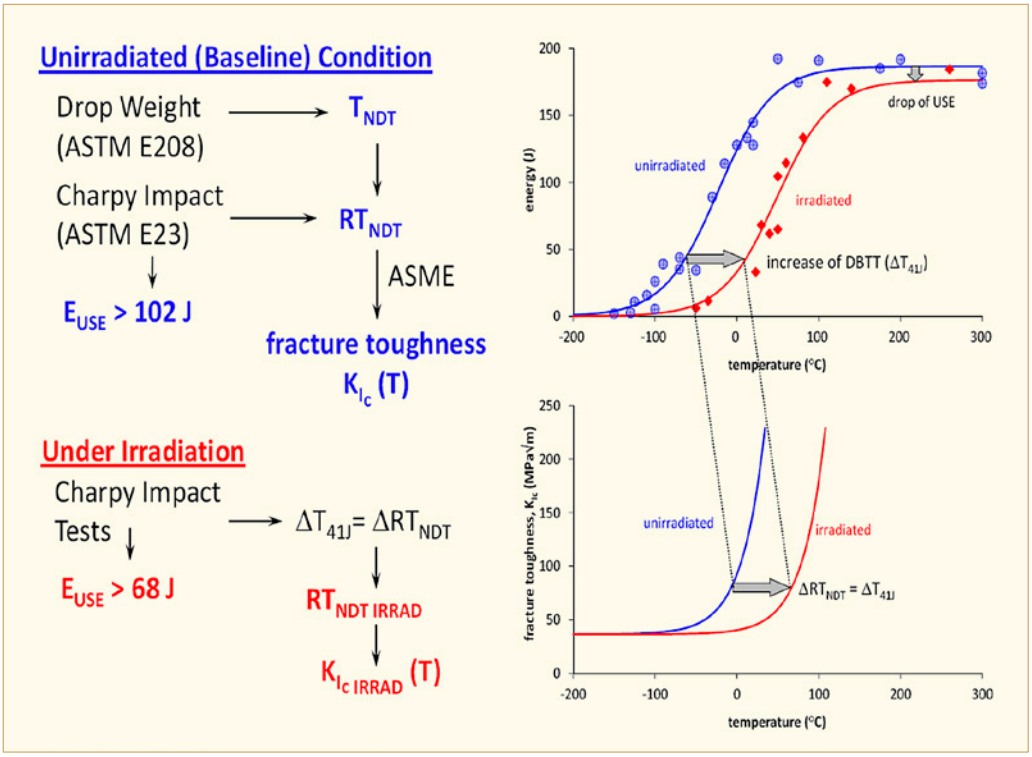

Figure 2-4: Procedure allowing the determination of the fracture toughness lower bound based on the T_{41J}-shift.

2.2.2 Irradiation effect

Four papers are dedicated to the irradiation effect on RPV steels.

The reference [Pineau & Landron, 2014] shows that the exploitation of tensile results allows expressing a relationship between yield strength increase and fluence value, as well as between strain hardening decrease and yield strength evolution. The use of these relations in the aim to predict the evolution of tensile properties with irradiation allows proposing a methodology to model entire stress-strain curves of irradiated base metal only based on the non irradiated stress-strain curve. These predictions are successfully compared with an experimental standard case in the paper. This approach may save a lot of time and resources as it decreases the need of hot cell mechanical testing of irradiated materials.

The amount of embrittlement of the base metal measured in the 4th surveillance capsule test of Genkai 1 showed larger transition temperature shift than the predicted value by the embrittlement correlation method of the relevant Japanese technical standards (JEAC4206-2007 and JEAC4201-2007). In order to understand the reason of the larger transition temperature shift in the base metal, and also to help improving the embrittlement correlation method of the Japanese relevant code, detailed microstructural characterization was performed using the base metals from the 3rd and 4th capsules of the Genkai 1 [Nakamuta et al, 2014]. The results obtained showed that the irradiation-induced microstructural changes in the Genkai 1 base metal were as expected by the model employed in the JEAC4201-2007 embrittlement correlation method; this standard was revised accordingly.

Opposite to typical western PWR weld metals, WWER-1000 RPV weld metals are characterized by a high content of nickel, mostly about 1.7 mass% with content of manganese around 0.8 mass% along with a very low copper content – about 0.05 mass% [Brumovský et al, 2014a]. In such material some late blooming phase[1] effect should be observed during irradiation. However, after irradiation at 290°C by five neutron fluence from 1.5 to 9.5×10^{23} m^{-2} (E>1 MeV), only low density of black-dot damage has been observed. It is assumed that most of defects are dislocation loops. The late blooming phases which may be observed from results of mechanical properties are probably below resolution of the used TEM, i.e. 1.5 nm.

Atom Probe Tomography has been used to characterize the microstructural evolution of three weld metals irradiated within the French RPV surveillance program at different doses, from 0.3 to 5.8×10^{23} $n.m^{-2}$ [Radiguet et al, 2014]. These materials were selected because their level of Ni and Cu allow highlighting the synergy between these two elements. APT revealed the presence of ~2-3 nm in diameter, roughly spherical, copper-, nickel-, manganese-, silicon-, and phosphorus-enriched solute clusters in all materials at nearly all the investigated neutron fluences. The average size of these solute clusters does not change significantly with neutron fluence whereas their mean chemical composition and number density increase with increasing neutron fluence. The comparison between the three welds revealed that the cluster size and composition are linked with the bulk composition and show a synergy between copper and nickel on cluster number density.

2.2.3 Flux effect

In the literature there are lots of contradictory data on the presence or absence, as well as the magnitude and the sign of "flux effect". The question whether material test reactor data can be used to supplement power reactor pressure vessel surveillance data is still debated in the international community and its implications are particularly important in the perspective of long term operation.

The reference [Gérard et al, 2014] states that, at high fluence levels, the flux effect on mechanical properties for both base and weld metals, is not significant, offering therefore the possibility of accelerated irradiation to investigate RPV embrittlement in the high fluence regime relevant for long term operation. In this work, the authors irradiated the low Cu base metal and weld of the Tihange-III surveillance coupon in the BR2 reactor at high flux. The BR2 flux is about two orders of magnitude higher than the flux in the surveillance position. Tensile, Charpy impact and fracture toughness tests were performed on both the surveillance and MTR specimens and compared to assess the neutron flux effect.

As opposed to the reference [Gérard et al, 2014] results, the reference [Gurovich et al, 2014] shows that for VVER-1000 RPV steels irradiated to comparable levels of fast neutron fluences with different fluxes, weld metal and base metal behave differently:

- There are structural prerequisites of flux effect under accelerated irradiation of weld metal samples with nickel content more than 1.35%, primarily due to differences in the kinetics of accumulation of grain boundary segregation at different irradiation fluxes, as well as due to some difference in contribution of radiation hardening and,
- There is no significant flux effect for base metal specimens (with Ni content < 1.35%) irradiated to fluence ~50×10^{22} m^{-2} with the difference in fluxes up to 200 times.

[1] There is experimental evidence that phases rich in Ni and Mn do form in irradiated low Cu steels. Because these phases may require a small degree of Cu precipitation to catalyse their nucleation, they may not contribute to hardening and embrittlement until relatively high fluences. These so-called "late-blooming phases" are responsible for a delayed embrittlement.

According to this work, direct use of results of the accelerated radiation for long-term prognosis of RPV weld materials embrittlement isn't correct. Thus, the reference [Erak et al, 2014] presents a method using the results of accelerated irradiation to justify the safe VVER -1000 RPV operation; this method takes into account the flux effects and temperature aging.

Opposite to references [Gérard et al, 2014] and [Gurovich et al, 2014], the reference [Soneda et al, 2014] found some flux effect on base metal irradiated in both surveillance capsules and a material testing reactor having higher flux. The Japanese study states that there might be a difference in ΔT_{41J} particularly at high fluences of high Cu materials. The response of the microstructure to different fluxes is complicated and material dependent. However, in general, the size of solute atom clusters becomes smaller and the number density becomes larger in higher flux irradiation. It is also interesting to see that the cluster size increases with fluence in surveillance materials, but it remains almost constant in the material testing reactor irradiated materials regardless of the bulk Cu content. There is also an effect of flux on the chemical composition. Ni content is slightly but consistently smaller in material testing reactor irradiated material. The reference [Soneda et al, 2014] concludes that these finding on the effect of flux are very useful to improve the model of embrittlement mechanism, and further modification of mechanism-guided embrittlement correlation method.

2.2.4 Master curve

In the reference [Barthelmes et al, 2014], the ductile to brittle transition reference temperature of RPV materials has been determined by two methods:

- Indirectly according to the RT_{NDT} concept by means of comparative examinations of irradiated and unirradiated notched-bar impact specimens and,
- Directly according to the Master Curve concept by means of examination of irradiated fracture mechanic specimens and determination of an alternative reference temperature RT_{T0}.

With the implementation and evaluation of the first irradiation surveillance program consisting of three sets, one unirradiated reference set and two irradiated sets, the safety of the RPV of the GKN II nuclear power plant could be proven for the assessment fluence of 8×10^{18} cm^{-2} (E>1 MeV) using the RT^{NDT} concept.

Against the background of a possible long term operation and the state-of-the-art of science and technology in 1998 the GKN II plant initiated a supplemental irradiation surveillance program with two irradiation sets containing fracture mechanic specimens for complementary proof of safety according to the Master Curve concept.

The reference [Viehrig et al, 2014] gives an example of the application of the master curve approach to the multi-layer beltline welding seam of Biblis C. The reference temperature, T_0, was determined for different thickness positions of the multi-layer welding seam. Additionally, the influence of the specimen orientation on T_0 was investigated. In contrast to the T-S orientation (crack extension through the thickness) the crack front of the T-L oriented specimens (crack extension in welding direction) penetrates several welding beads. By means of fractographic and metallographic analyses it was shown that the distribution of the crack initiation sites is not necessarily correlated to the structure of the different welding beads along the crack front. Furthermore, it was found that the scatter of the K_{Jc} values determined with T-S specimens is significantly higher than in case of the T-L specimens. T_0 values measured at different thickness locations of the multi-layer welding seam vary in a range of about 40 K.

2.2.5 Long term operation

The possibility of extending the operational life of reactor pressure vessels up to 80 years presents the problem of the availability of materials irradiated at high neutron fluence and low neutron flux. The ability of the existing trend curves to predict high fluence embrittlement is a question of debate, and a critical analysis of these curves should be based on a consistent microstructural examination of irradiated materials. Within the LONGLIFE 7FWP, neutron irradiated RPV materials, relevant for long term operation, some of them coming from surveillance programs, have been characterized by means of a combination of microstructural techniques and mechanical tests. In the reference [Serrano et al, 2014], the analysis of the links between microstructural features (solute nanoclusters, dislocation loops and voids) and hardening and embrittlement measurements by mechanical testing, is presented. Current hardening models, based on the contribution of precipitates, or nanoclusters, seem to underestimate irradiation hardening for very high fluences, mainly when matrix damage (dislocation loops) is observed. Regarding chemical composition effects, the predominant role of Ni and the synergism between Ni-Mn and Si are also identified. Low-Cu alloys show a threshold value of radiation induced features to produce an effect on mechanical properties which calls for further in-depth analyses.

The reference [Hein et al, 2014] presents some practical implications for RPV irradiation surveillance under LTO conditions which are based on results of experimental examinations on representative irradiated RPV steels. While the impact of chemical composition (copper and nickel) on irradiation embrittlement and the most important mechanisms such as formation of element specific precipitations, segregations, and matrix defects are well known in relation to the change of material properties, other issues such as the flux effect, the occurrence of late irradiation effects, and the reliable application of embrittlement trend curves need further clarification. In this context the identification and assessment of uncertainties of RPV irradiation surveillance data are important for future research to ensure safe LTO referring to RPV integrity of LWR.

An alternative but complementary surveillance program assessment was developed in Belgium, the so-called enhanced surveillance, in order to benefit from the latest developments in the area of materials science and irradiation effects. By combining few additional experimental tests and multiple property correlation supported by analytical analysis tools, the data can be assessed in a much more consistent way than solely relying on the Charpy impact test and empirical correlations. The reference [Chaouadi & Gérard, 2014] presents the whole procedure with the support of relevant examples and highlights the benefits of such an approach in enhancing the confidence in the surveillance results and in demonstrating the existence of additional safety margins with respect to the regulatory approach.

2.2.6 Warm prestress

Warm prestress seems to be a French concern as only French research organisations have presented papers dealing with this issue.

Fracture toughness is required for assessing structural integrity of reactor pressure vessels. It has been long recognized that load history with material cooling can increase the effective toughness while conventional toughness is considered as decreasing in basic rules, leading to over pessimistic assessment in case of cooling transient. The so-called Warm PreStress effect corresponds to the absence of brittle crack propagation after prestressing if the load is held constant or decreased as the temperature is decreased, even if the toughness of the material is exceeded. In the case of life extension, such thermomechanical transients may become relevant for irradiated RPV in case of hypothetical Loss of Coolant Accident. The reference [Hure et al, 2014] investigates the WPS effect on A508 Cl3 RPV steel, irradiated up to a maximal fluence of 13×10^{19} n.cm^{-2} (E>1 MeV) at a temperature of 288°C in Osiris Material testing Reactor, which corresponds to more than 60 years of operations in a French Pressurized Water Reactor. The unirradiated and irradiated materials have been characterized through tensile, Charpy V-notch and Compact Tension tests, yielding the evolution of the material properties with neutron irradiation. Various types of thermomechanical loadings have been performed on precracked compact tension specimens, all of them confirming the WPS effect. The increase of the effective toughness after warm prestressing is shown to be in agreement with the predictions from engineering based models.

The second paper [Landron et al, 2014] confirms the beneficial effect of WPS on the cleavage fracture resistance of the irradiated materials. No fracture occurred during the cooling phase of the loading path and the fracture toughness values are higher than that measured with conventional isothermal tests. The analyses of the experiments, conducted using either simplified engineering models or more refined fracture models based on local approach to cleavage fracture, are in agreement with the experimental results.

2.2.7 Thermal ageing

With life extension, thermal ageing is a growing concern, shared by several countries. The 3 papers dealing with this issue are from 3 different countries (Japan, Russia and France).

Embrittlement correlation methods for irradiated reactor pressure vessel steels have been developed world-wide to predict the amount of embrittlement during plant operation. Effect of chemical composition is considered in such embrittlement correlation methods. However, the very fundamental process of solute atom behavior during solute atom cluster formation is not fully understood. In the reference [Nomoto et al, 2014], thermal ageing experiment of RPV model alloys was performed in order to obtain information on the effect of chemical composition on the hardening. The effect of additional element to Fe-Cu model alloys was studied. Addition of Ni or Si alone does not have clear effect in this study. Addition of Mn to Fe-Cu-Ni alloy accelerates the cluster formation and hardening drastically. The effect of composition on the cluster strength is not clear. Comparison between the microstructure and increase in hardness of the model alloys needs careful consideration. Hardening before peak hardening has linear correlation with APT data.

The VVER-1000 thermal aging surveillance specimen's sets are located in the reactor pressure vessel under real operation conditions. Thermal aging surveillance specimen's data are the most reliable source of information about the evolution of VVER-1000 RPV materials properties because of long-term (hundred thousand hours) exposure at operation temperature. The yield strength data, study of carbides evolution show absence of hardening effects due to thermal aging at 310–320°C. Measurements of phosphorus content in grain boundaries segregation in different states have been performed. The correlation between intergranular fracture mode in Charpy specimens and transition temperature shift under thermal aging at temperature 310–320°C is presented in the reference [Chernobaeva et al, 2014]. All these data allow developing the model of thermal aging.

3 Pressure vessel

3.1 Irradiation effect

The principle of RVSP is based on the use of tensile, impact strength and sometimes toughness specimens taken and machined during the manufacturing process of each core vessel. Then, these specimens are put into irradiation capsules, which are placed near the core. These capsules, extracted at various step of the reactor life-cycle and positioned closer to the fuel assemblies than the shell internal surface, receive a higher neutron flux than the reactor vessel material, which makes it possible to anticipate the damage undergone by irradiation and to estimate the conservatism of predictions. The results obtained represent the shell state under irradiation after approximately 10, 20, 30 and 40 years of operation.

In order to quantify the embrittlement due to irradiation, Charpy tests are performed to determine the ductile-brittle transition temperature shift due to irradiation, for each capsule of RVSP. Moreover, results from these tests are compared to a semi-empirical formula, which predicts the shift of transition temperature as a function of fluence and embrittlement-involved chemical elements.

The reference [Pineau & Landron, 2014] is focused on the analysis of tensile tests results for base metal specimens, since the beginning of French RVSP. It appears that tensile data are rarely used in the monitoring of irradiation effect although they highlight an increase of yield strength ($Rp_{0.2}$) and a decrease of strain hardening due to irradiation.

In French RVSP, surveillance tests data are collected from the tensile tests at 20°C and 300°C for the non-irradiated material, just after the manufacturing process and only at 300°C for the irradiated material. Base metal tensile specimens, used to surveillance tests are taken in two samples of the monitored vessel shells, in the forging direction. From plants manufacturing, tensile specimens are taken from each part of the ¼ of shell thickness, on 4 levels of the acceptance ring height.

The tensile tests results can be analyzed to study different issues:

- The existence of a thermal effect during fabrication due to variability of quench velocity in the acceptance ring for some monitored vessel shells;
- The comparison between hardening and embrittlement due to irradiation to propose a relationship;
- A proposition to model the decrease of strain hardening and to combine these two models to predict the stress-strain curve of irradiated base metal.

The effect of irradiation on stress-strain curves is illustrated in Figure 3-1 at 300°C for a core shell of a French power plant. Again, an increase of the yield strength and a decrease of the strain hardening are observed. The appreciation of the behavior law of a material is particularly important, especially in case of finite element simulation where the best description of the material behavior is necessary for the accuracy of results. However, tensile tests on irradiated specimens require adapted devices in particular working in hot laboratory. An alternative to experimental testing would be a modeling of the stress-strain curve of the irradiated material deduced from the curve obtained in unirradiated condition.

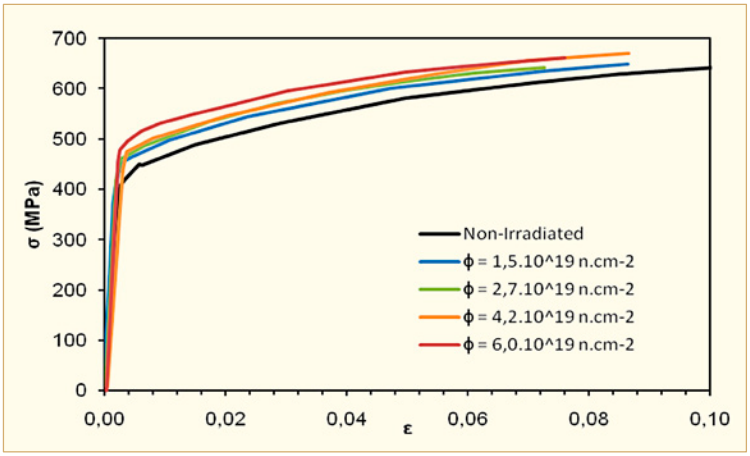

Figure 3-1: Tensile curve evolution of irradiated base metal (at 300°C).

Such a methodology has been implemented using the following proposition:

Eq. 3-1:
$$R_I(p) = (Rp_{0.2})_I + \frac{n'_I}{n'_{NI}} \cdot \left(\frac{dR}{dp}\right)_{NI} dp$$

where: R(p) = tensile stress; n'_I = pseudo strain hardening coefficient for irradiated base metal; n'_{NI} = pseudo strain hardening coefficient for non-irradiated base metal and p = plastic strain.

The irradiated stress-strain curve is obtained from the slope of the non-irradiated stress-strain curve and the pseudo coefficient ratio which prediction with the fluence is given in the previous paragraph. Use of the pseudo coefficients ratio as the multiplication factor takes into account the reduction of strain hardening induced by irradiation.

In this study, the proposed modelling is applied on a standard case that the evolution of tensile properties following the models proposed in the previous paragraphs. Evolutions of $\Delta Rp_{0.2}$ and n'_I/n'_{NI} with the fluence are given in Figure 3-2.

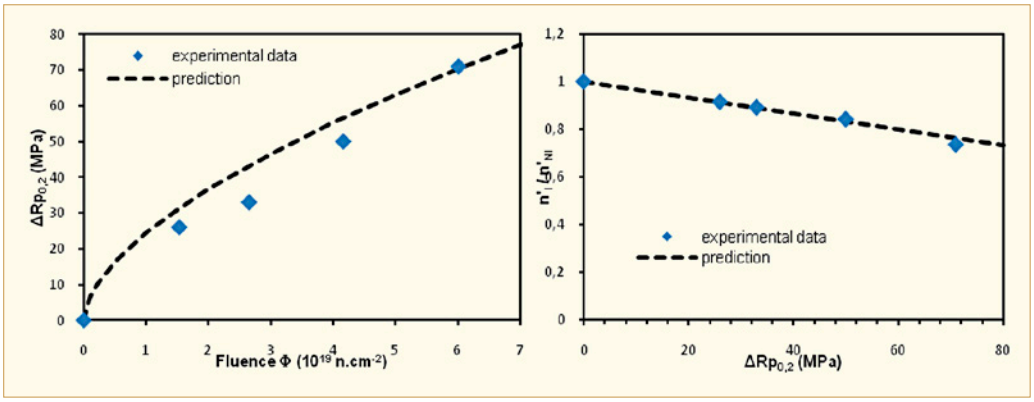

Figure 3-2: Comparison of the measured evolution of $Rp_{0.2}$ and n'_I/n'_{NI} with the predictions for the selected material.

To predict the stress-strain curve at irradiated state, Eq. 3-1 is employed with:

- $(Rp_{0.2})_I = (Rp_{0.2})_{NI} + \Delta Rp_{0.2}$ using equation $\Delta Rp_{0.2}^{300°C} = k \cdot \Phi^{0.59}$ (where k = 24 is a constant value and Ø the measured fluence value) to predict $\Delta Rp_{0.2}$ with the fluence,

- the prediction given by equation $\frac{n'_I}{n'_{NI}} = 1 - \frac{\Delta Rp_{0.2}}{\alpha}$ for $\frac{n'_I}{n'_{NI}}$
  where α = 300, the best fit value estimated with RVSP data,
- the stress-strain curve from non-irradiated material to determine $\left(\frac{dR}{dp}\right)_{NI}$.

The prediction of irradiated stress-strain curve is then achievable only using the stress-strain curve from non-irradiated material that is easily known. This methodology is tested on the standard case presented in Figure 3-2 and Figure 3-3 for the four levels of fluence for which experimental data were available. Comparison between experimental stress-strain curve and predictions is given in Figure 3-3. There is a quite good agreement between experiments and predictions at low fluence: the predicted tensile curves are really close to the experimental ones. At higher fluence, the predictions produce lower values than experimental tests in particular at large plastic strains. However, values given by the prediction are still suitable with respect to experiments.

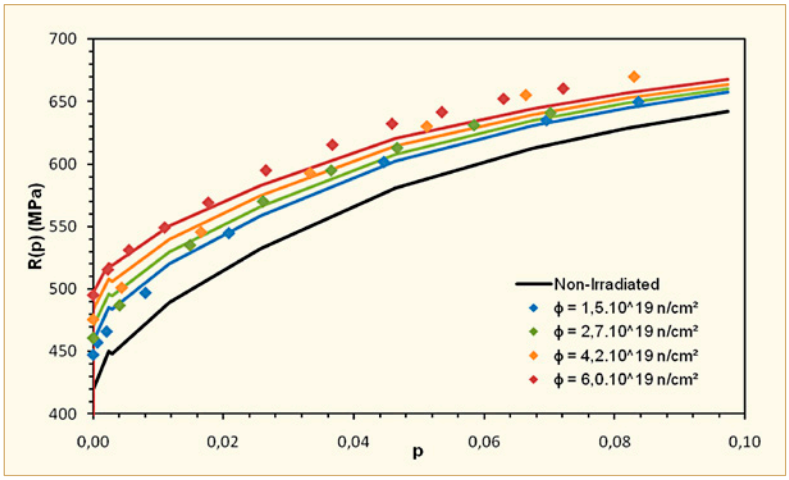

Figure 3-3: Assessment of the prediction on experimental data (dots are for experimental data and lines for predictions).

The surveillance program to evaluate the neutron irradiation embrittlement of RPV steels of the commercial nuclear power plants in Japan is specified in the Japan Electric Association Code, JEAC4201-2007. This code defines the withdrawal schedule of surveillance capsules, the experimental details of Charpy impact test and tensile test, and the method to calculate the amount of embrittlement for a given condition (embrittlement correlation method).

Following the specification of JEAC4201-2007, the 4th surveillance capsule of Genkai Unit 1 of Kyushu Electric Power Company in Japan was withdrawn in 2009 and tested in the successive years. Genkai Unit 1 is a two-loop pressurized water reactor with an electric capacity of 559 MWe. This plant has been in commercial operation since October 1975. From the result of the 4th surveillance test, it was found that the amount of embrittlement of the base metal, which is the limiting material of this plant, shows a larger shift than the value predicted by the embrittlement correlation method of JEAC4201- 2007. Therefore, an additional margin was added to the predicted values, and this conservative prediction was used in the structural integrity analysis of the RPV of Genkai Unit 1. In parallel to the structural integrity assessment, efforts were devoted to identify the reason of the larger amount of embrittlement than the JEAC4201-2007 prediction particularly from the microstructural (or mechanism) point of view.

In the reference [Nakamuta et al, 2014], the surveillance test results of Genkai Unit 1 are presented, followed by the results of the structural integrity analysis of the RPV. Then the results of microstructural characterization are demonstrated to show that there is no anomaly in terms of the irradiation induced nano-features.

4 Pressure vessel internals

4.1 NonDestructive Examination

The Electric Power Research Institute's Materials Reliability Program has developed an Inspection and Evaluation (I&E) Guideline (MRP-227A) to meet the requirements for aging management of pressurized water reactor vessel internals and license renewal activities. To support the guidelines MRP has also developed an Inspection Standard (MRP-228, Rev 1) that provides the requirements for the nondestructive examinations. The reference [Spanner, 2014] describes the NDE procedure, equipment and personnel requirements included in the Inspection Standard. The inspection of vessel internals will be a necessary component of a plant's License Renewal and become a regulatory commitment. Generally, visual examinations will be used to detect evidence of age related degradation mechanisms but ultrasonics are used to examine bolting. During development of the I&E Guidelines several components have been identified as being potential areas to consider for inspection. Most of these components are susceptible to damage mechanisms that are not typically included in a nuclear in-service inspection program for the pressure boundary components and these are addressed in the Inspection Standard. (Figure 4-1) The Inspection Standard describes NDE procedure requirements for visual and ultrasonic examinations. It also describes demonstrations that have been conducted for the ultrasonic examination of bolts.

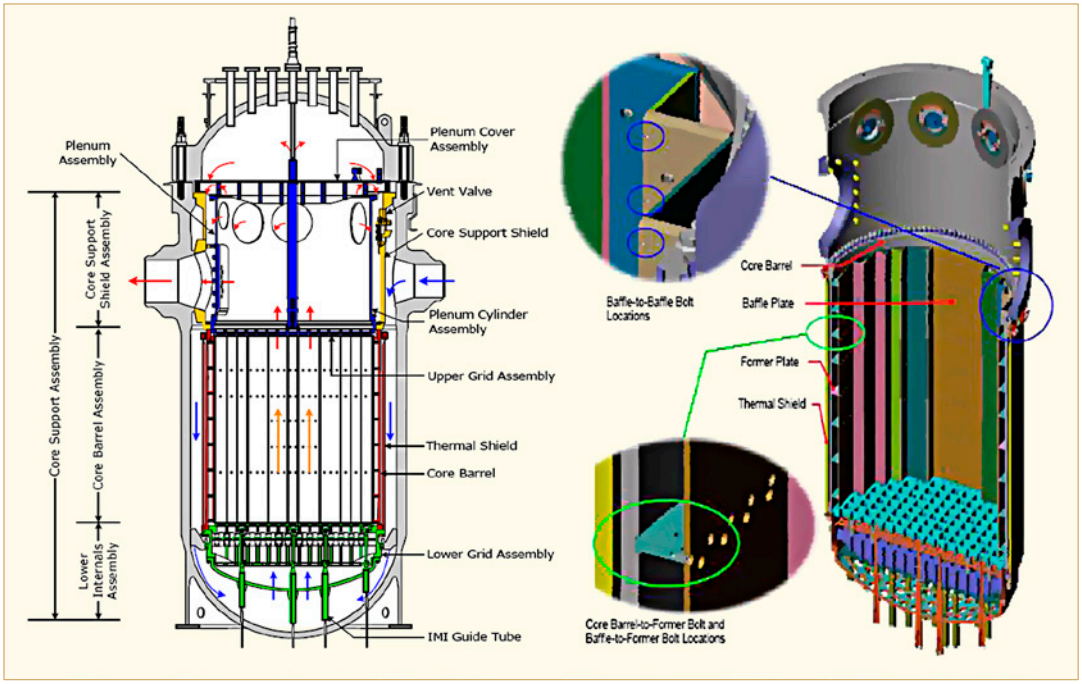

Figure 4-1: Internals baffle and former plates.

The process for NDE system qualification described in this paper is based on the use of technical justifications as described in the American Society of Mechanical Engineers Boiler and Pressure Vessel Code, Section V, Article 14 and is similar to the European Network for Inspection Qualification. The technical justification is a detailed explanation of the procedure including the method, and any laboratory or field experience that support the procedure capabilities. The technical justification provides the technical basis and rationale for the qualification. This qualification process builds on the field experience and previous work performed by the inspection vendors and other inspection organizations to develop the examination systems already in use today throughout industry and does not mandate any new performance demonstrations. Where there is a need to simulate performance specific examinations for the purpose of preparing the technical justifications required by the Inspection Standard, or for other reasons, such as to qualify improved techniques, new or existing vendor mockups may be used or, where mockups of such components are not otherwise available, mockups developed by the MRP may be used.

The general procedures describe the requirements for NDE system qualification, use of mockups, and general requirements for visual and ultrasonic examination for reactor vessel internal components. A NDE system is generally defined as the procedure, personnel, and equipment used to perform a NDE examination. The term NDE system is applicable for any method of examination, including visual inspection. The general procedures provide a uniform approach for NDE system qualification and consistency in the application of examination methods.

The technical justification is a required written report providing the detailed explanation of the examination process, including the theory of the examination technique as applied to reactor internals inspections, the essential variables of the procedure, other influential parameters important to the overall performance of the examination system, and field experience and/or mockup demonstrations supporting the capabilities of the NDE system. The technical justification includes a description of the active or anticipated material damage mechanisms and the NDE evaluation process used to interpret the results of the applied examination technique. Prior to use of an NDE system for reactor internals inspections, the technical justification report shall be reviewed and approved by the utility.

The content of the technical justification shall be as follows: (1) description of the component(s) and degradation mechanism(s), (2) general description of the NDE system, (3) influential parameters important to the overall examination performance, including the essential variables of the procedure, (4) description of the examination technique, and (5) description of procedure experience.

So far, six PWR plants in the USA have completed inspections of their internals using the I&E Guideline (MRP-227) and the Inspection Standard (MRP-228). One of these inspections is summarized in the paper presented hereafter. Examination results show few instances of service-induced degradation flaws, as expected. The few instances of degradation have mostly occurred in bolting.

The reference [Davidsaver et al, 2014] describes an application of the Inspection and Evaluation Guideline MRP-227A.

Duke Energy and AREVA overcame a significant technology and NDE challenge by successfully completing the first-of-a-kind MRP-227-A scope requirements at ONS-1 in one outage below the estimated dose and with zero safety issues or events while simultaneously performing two other major RV in-service examination scopes (Figure 4-2).

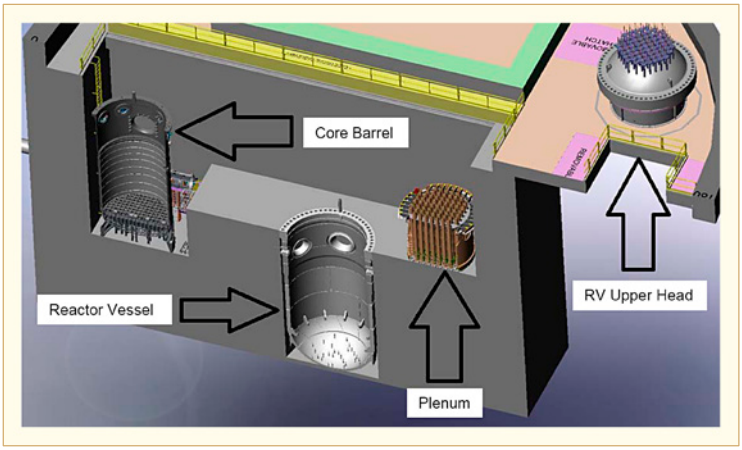

Figure 4-2: General arrangement of Oconee Unit 2 Fall 2013 Refueling Outage RV Examination Activities.

This performance was repeated at ONS-2 a year later. The scope undertaken during the ONS-1 and ONS-2 outages represents some of the largest RV inspections performed in the PWR industry to date. Since the technical justifications for the UT examinations were so useful to the personnel performing the examinations, Duke Energy elected to create technical justifications for component items receiving visual examinations as well.

Replacement of the vent valve and the lack of any significant degradation observed on the remaining component items provide confidence that the RV internals will be able to perform their safety-related functions during the period of extended operation (Figure 4-3).

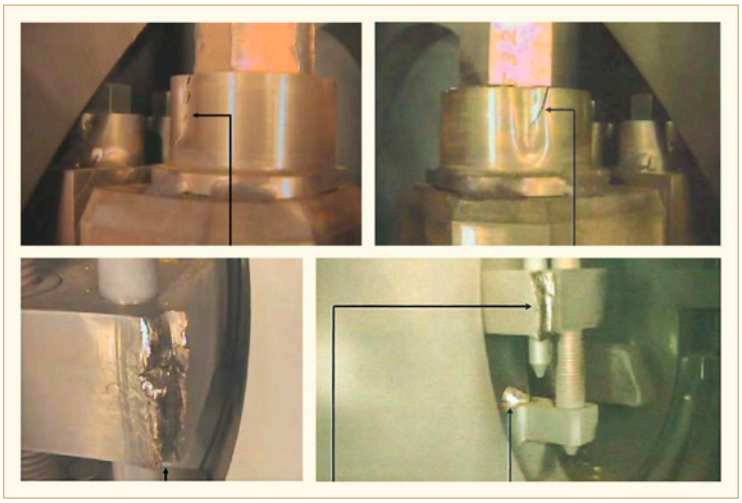

Figure 4-3: Visual examination video capture of the ONS-2 core support shield vent valve. Top left: jackscrew locking crimp cup indication, item #1. Top right: jackscrew locking crimp cup indication, item #2. Bottom left: body impact damage. Bottom right: body impact damage and barrel nut incorrect positioning.

The remote NDE tooling and processes developed to examine the MRP-227-A scope for ONS-1 and ONS-2 are transferable to other PWRs. The lower core barrel and flow distributor bolt tooling, SUSI spider tool, and the CRGT inspection tool and their associated inspection techniques and procedures are all directly transferrable to B&W design units (Figure 4-4). The baffle bolt inspection tooling concepts and processes are also directly transferable to all PWRs.

5 Stainless steel corrosion

5.1 Operating experience

Stainless steels are widely used in Fast Breeder Reactors cooled by sodium (see Table 5-1).

Table 5-1: Stainless steels used in French sodium FBRs.

Structures & components	Operating temperature	Phénix SSs	Superphénix SSs
Primary circuit	380–560°C	316, 316L, 316Ti	316L, 316LN, 304L, 304LN
Secondary circuits	350–550°C	304, 321, 316L	316LN
Steam generator	245–510°C (water side)	Heater & superheater: 321	SG tubes: Alloy 800
			ANT International, 2015

Although they exhibit very satisfactory compatibility both with sodium in primary and secondary circuits and with water vapor on the steam generator water side under normal operation, stainless steels can show susceptibility to different corrosion mechanisms particularly following accidental situations (leading to pollution) or during maintenance operations. The corrosion phenomena that could be encountered in a sodium cooled reactor under normal operation (including nominal, transient conditions and shutdown), maintenance operations (cleaning, decontamination) or accidental situations (sodium-water reaction, sodium leak, air ingress) are identified in Figure 5-1.

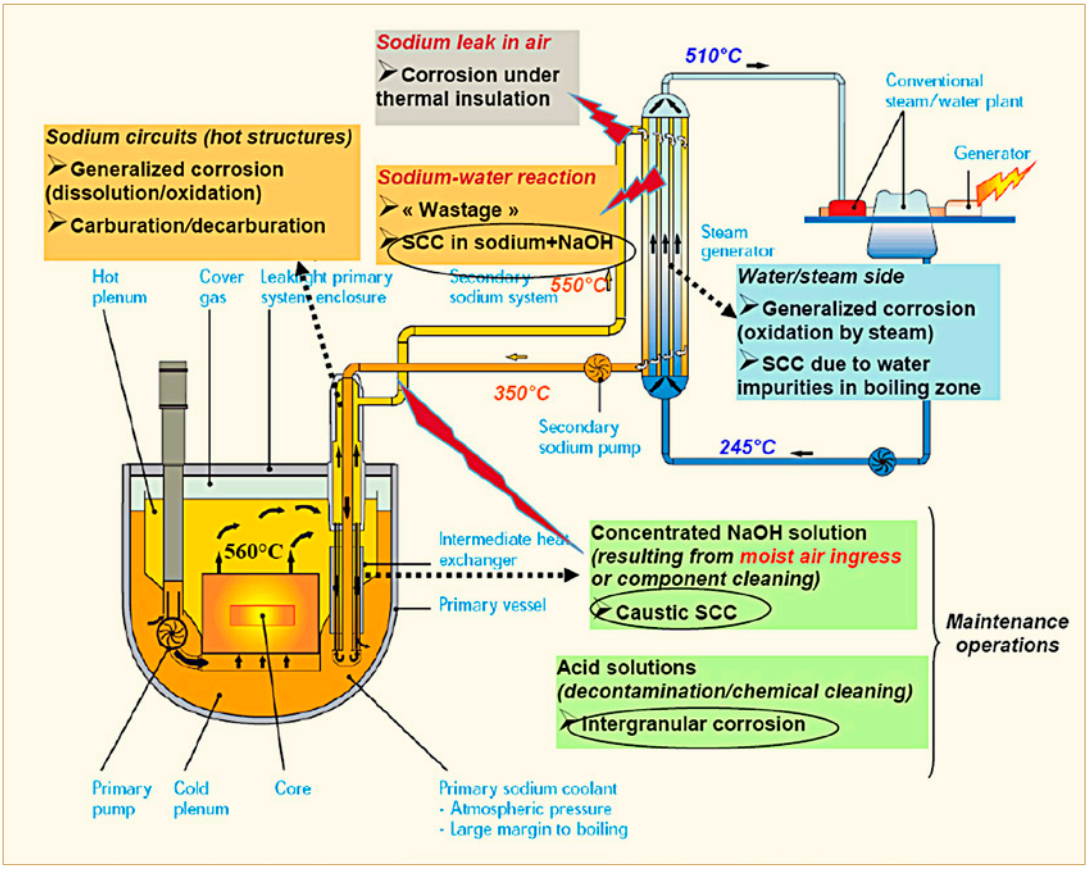

Figure 5-1: Potential corrosion risks in sodium cooled FBR.

The reference [Grabon et al, 2014] is focused on the most threatened corrosion mechanisms specific to the use of sodium at high temperature as coolant in FBR - apart from "wastage" - :

- SCC induced in sodium polluted by sodium hydroxide (following sodium-water reaction or incomplete cleaning of component);
- SCC induced by caustic solution during maintenance operations (cleaning of component or repair on drained sodium circuit inducing moist air ingress);
- IGA induced by acid solutions used during maintenance operations (decontamination of component, chemical cleaning).

Corrosion risks only appear if some conditions related to material factors, chemical environment and operating conditions exist simultaneously as shown in Figure 5-2.

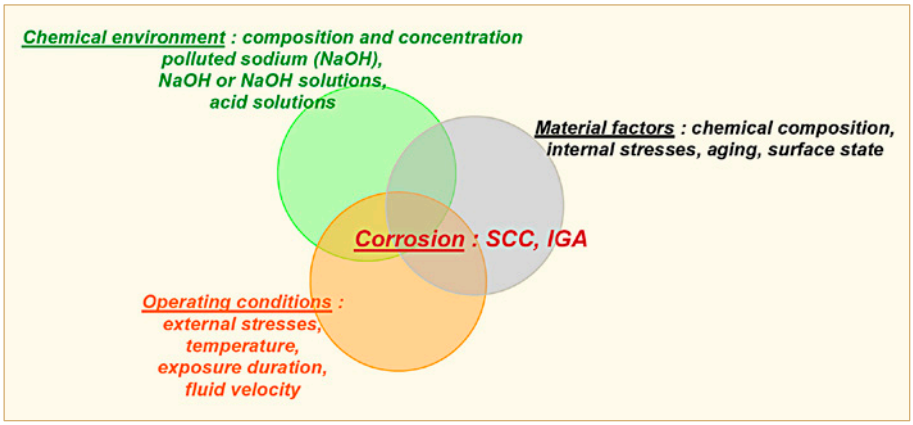

Figure 5-2: Conditions leading to corrosion.

Then, the paper describes the various mechanisms and conditions leading to corrosion and illustrates them with some examples of corrosion encountered through Phénix experience (1974–2009) or in CEA sodium loops. The solutions and the preventive measures that have been put in place in the form of design rules and operating procedures are mentioned. Generally the plant operator cannot control the material parameters (metal composition, aging, stress) during the lifetime of the facility. Thus most of the time preventive measures consist in excluding at least one of the two other following factors related to:

- The chemical environment (technical rules to avoid air ingress during repair, elimination of the potential aqueous phase of sodium hydroxide before preheating of drained sodium circuit, elimination of residual sodium hydroxide by sodium purification before restart-up, definition of adequate solution for cleaning or decontamination operations taking into account the sensitization state of the material and welds, elimination of enclosed zones by optimized design and draining of sodium for example);
- And/or the operating conditions (temperature, duration of exposure during transient or following accidental situations and during maintenance operations) when the environmental conditions are not under control (NaOH solution concentration during cleaning operation or in case of accidental water or moist air ingress into sodium circuit).

Moreover corrosion of the primary components during cleaning and decontamination operations before repair had to be carefully examined to authorize their reuse in the reactor. All the removable components, specially primary and secondary pumps and intermediate heat exchangers, have been successfully cleaned, decontaminated and repaired when necessary then reused in the reactor. Moreover the 47 modules of the SG have been re-started up in 2003 after cleaning and repairing.

In 2005, during a recurring in-service inspection (visual inspection) of the core barrel bolts in a German PWR, crack like indications were detected on four barrel bolts, (see Figure 5-3). The bolts, known as star bolts, are made of SS type 316 Ti (German material # 1.4571) bars, which are cold worked to adjust the required mechanical properties. In the following due to additional inspection all six operating Siemens/KWU PWR plants with mounted core barrel and star bolts were affected. Therefore a research program was launched by AREVA and VGB to systematically investigate the root cause of these failures. Beside laboratory investigations of cold worked austenitic stainless steel under PWR primary environment, engineering work was initiated to compile and analyze the data from field experience. The reference [Kilian et al, 2014] presents the results of the engineering work.

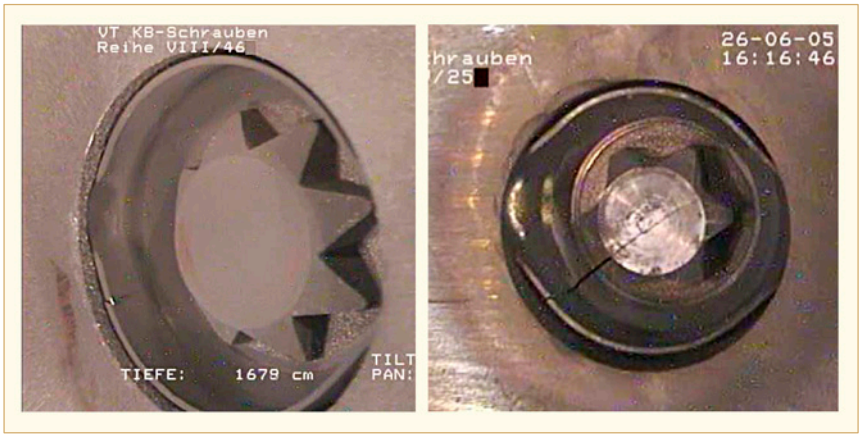

Figure 5-3: Crack like indication on a barrel bolt. Left: in the area of cup preventing unintentional loosening. Right: crack initiation in the head.

The core baffle surrounds the polygonal shape of the reactor core, and is bolted to the core barrel via the formers without welded connections, see Figure 5-4. The design of the core shroud must ensure that the forces and stresses occurring during operation are safely under control. The basic elements of the core shroud in PWR Plants designed by SIEMENS/KWU are the vertically oriented baffles, several levels of horizontally oriented formers and the baffle-former bolts. Two types of fasteners are used: long (external) barrel former bolts (140 mm) that connect the formers to the core barrel, and short (internal) baffle former bolts (47 mm) connecting the formers to the baffles. The latter ones may also be referred to as core shroud bolts. The formers and baffles are made of material type AISI 347 stainless steel (German Material # 1.4550 mod., C = 0.04 wt%, Nb = 0.65 wt%, Nb/C≥13), as are the vast majority of the other RPV-Internals.

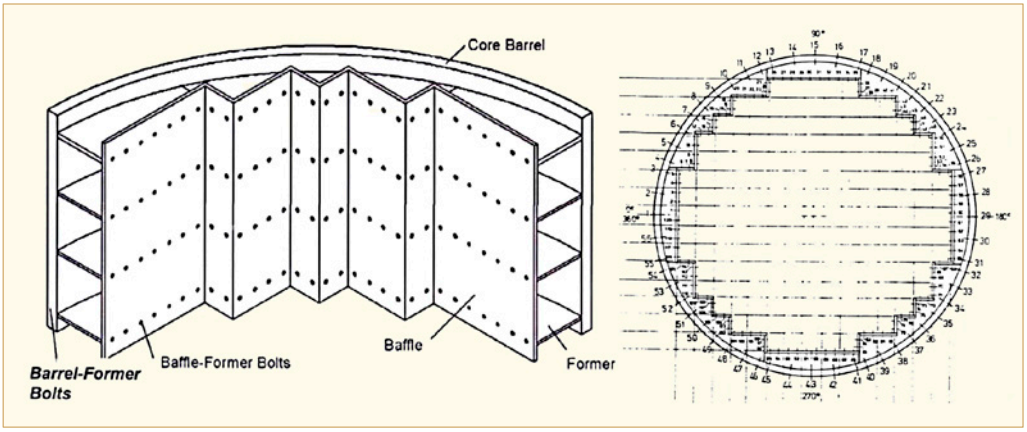

Figure 5-4: Left: bolted design of the core baffle; right: top view of core barrel with core baffle.

6 Nickel alloys corrosion

6.1 Destructive examination, X-750

During an in-service inspection performed as part of the March 2010 D.C. Cook Unit 1 refueling outage, 7 of 48 clevis bolts and 1 of 8 dowel pins in the Lower Radial Support System were observed to have visual indications of bolt failure. The LRSS supports the lower reactor internals and consists of six support locations equally spaced around the bottom circumference of the reactor vessel just above the lower head. There are six clevis keyway locations on the interior of the reactor pressure vessel that are numbered sequentially around the circumference at 0°, 60°, 120°, 180°, 240°, and 300°. Each support location consists of two lugs welded to the interior of the reactor vessel. A clevis insert is installed on each pair of lugs and constrained by an interference fit. Each clevis insert is fastened by eight clevis bolts and two dowel pins. The eight bolts are arranged in a vertical line of four bolts on each side of the clevis insert, separated into groups of two – high and low – by a dowel pin. For purposes of the laboratory analysis, the bolts were referred to as high left (bolts 1 and 2), low left (bolts 3 and 4), high right (bolts 5 and 6) and low right (bolts 7 and 8). The reactor vessel side of the LRSS arrangement, including the bolt numbering convention, is shown in Figure 6-1.

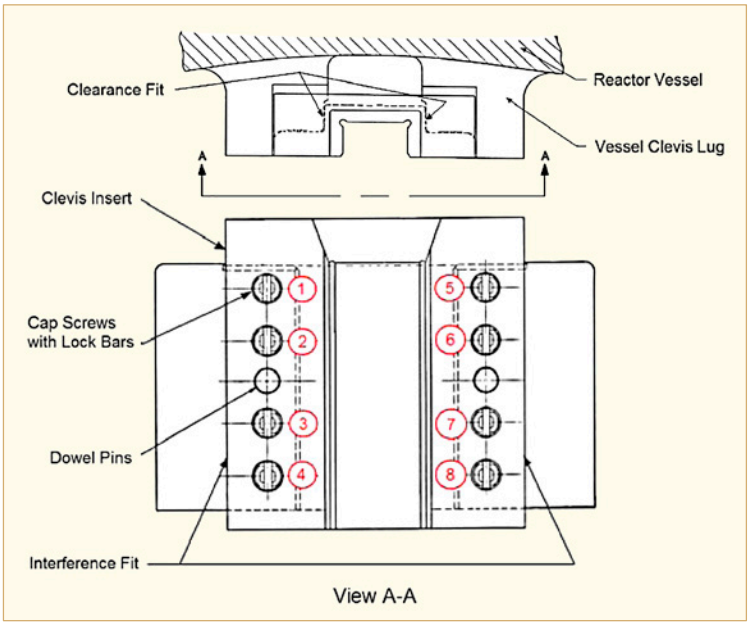

Figure 6-1: Schematic diagram showing locations of clevis lug, insert plate, and clevis bolts.

Mating radial keys are installed on the core barrel, which interface with the clevis inserts when the lower internals are installed. The original clevis insert bolts are socket head cap screws with a slot in the head to accommodate a welded lock bar. Underwater images of a clevis lug, clevis insert, broken bolt, and intact bolt taken during the March 2010 inspection are presented in Figure 6-2. The clevis bolts were fabricated from Alloy X-750 (UNS N07750) material. The reported heat treatment for the bolts included a low solution annealing temperature (<982°C) and a two-step aging treatment. Alloy X-750 material heat treated in this manner is known to have poor resistance to IGSCC in both high and low temperature primary water. A minimum pattern of clevis bolts was replaced in all six clevis inserts during the spring 2013 Unit 1 refueling outage, including all with visual indications. A total of 29 clevis bolts – 16 broken and 13 intact – were removed from the LRSS. Broken bolts, or a combination of broken and intact bolts, were removed from four of the six clevis inserts, while bolts removed from the remaining two clevis inserts were all intact. All 29 bolts were shipped to the Babcock & Wilcox Lynchburg Technology Center for comprehensive laboratory analysis and testing [Hyres et al, 2014].

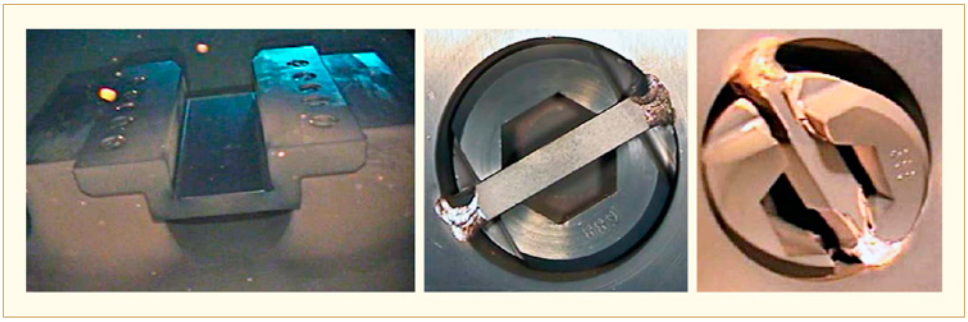

Figure 6-2: Underwater images of clevis lug and insert plate (left), intact bolt (middle), and broken bolt (right).

Visual and stereomicroscope examinations show that of the 29 clevis bolts, 16 bolts had fractured at the head-to-shank transition and were received in two pieces. The remaining 13 bolts were received intact (in one piece); however, all were later determined to be cracked around the circumference at the head-to-shank transition based on the stereomicroscope examinations. Most of the intact bolts exhibited a typical cracking pattern consisting of a straight, unbranched crack for approximately half of the circumference, while the other half comprised many angular cracks that may or may not have linked up. The angular cracks were oriented in a right hand helical pattern around the circumference of the bolt. Broken bolts exhibited a similar pattern when observing crack elevation variations around the bolt OD in the head-to-shank transition.

Stereomicroscope examination of the fracture surfaces on the broken bolts identified multiple crack initiation locations around the bolt circumference at the head-to-shank transition. Most of the bolt fracture surfaces exhibited a clear axis of symmetry, as shown by the dashed red lines in Figure 6-3. The symmetry appears to be the result of two diametrically opposing crack fronts propagating toward each other before linking up near the center of the bolt section. For each bolt, the orientation of the axis of symmetry was compared with the location and orientation of each bolt within the clevis insert plates, and no correlation was found. This suggests that that the stresses driving crack initiation and propagation were predominantly from the bolt installation preload, and not from forces on the bolts during plant operation (e.g., thermal expansion, bending) or the result of a non-perpendicularity of the bolt seating surfaces with respect to the bolt holes in the insert plates.

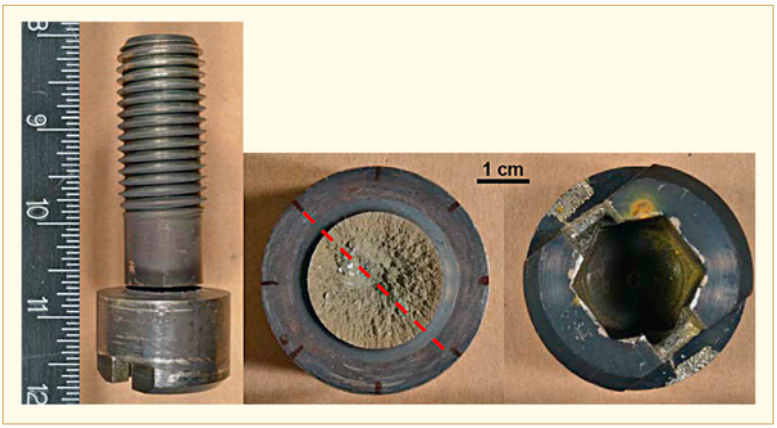

Figure 6-3: Bolt 120°-6 side view (left), open fracture showing lighter macro appearance (center), and opposite side of head (right). Bolt head photos match in-service position.

Two broken and two intact bolts were selected for the destructive analysis and testing based on the visual and stereomicroscope examination results. The selected bolts were located in three of the six clevis locations and included two bolts from the 120° clevis, which experienced the greatest population of in-service bolt failures (all 8 bolts failed).

SEM fractography of the two broken bolts (120°-2 and 120°-6) and one intact bolt (240°-7) identified that cracking was essentially 100% intergranular with very small, isolated regions of transgranular cleavage or ductile tearing near the center of the bolt section where final fracture occurred.

Optical and SEM metallography of the four selected bolts showed that multiple intergranular cracks, typical of IGSCC in PWR primary water, initiated around the circumference of each bolt at the head-to-shank transition and propagated inward toward the bottom of the hex socket (Figure 6-4 top). The resulting crack surface formed was conical with the conical plane at approximately 35° to the bolt seating surface. The crack initiation and propagation direction coincided with maximum local tensile stress in the area. Cracking exhibited a branched intergranular morphology in all areas examined (Figure 6-4 bottom).

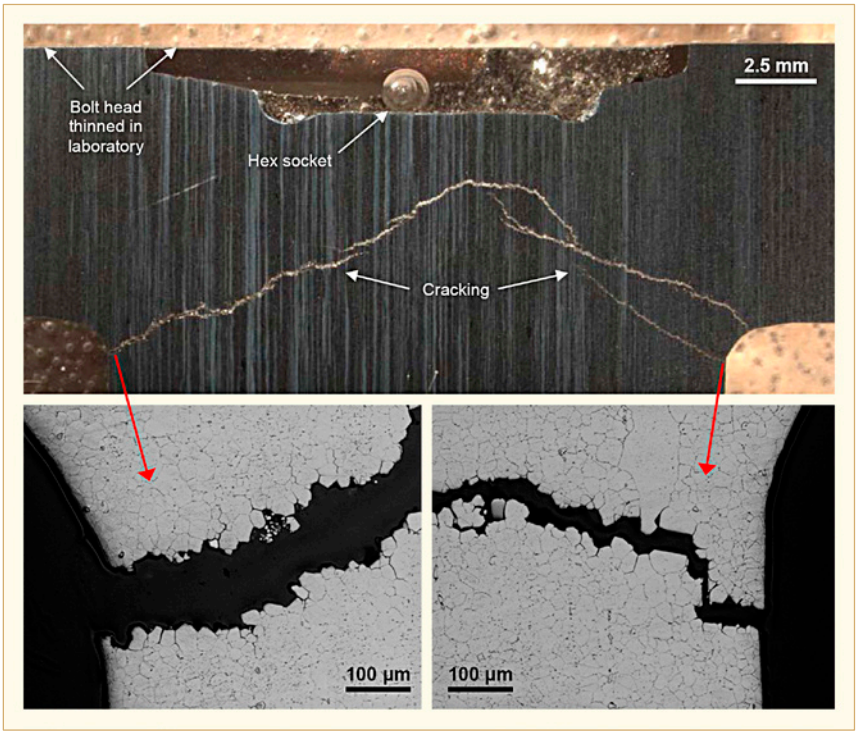

Figure 6-4: Top: 240°-7 bolt head cross section showing banded microstructure; bottom: close-up of intergranular cracking in the head-to-shank transition areas.

The microstructure of Alloy X-750 in the reported heat treatment is expected to contain second phases such as carbides, intermetallics, and nitrides in a relatively fine-grained matrix. The carbides are mostly MC-type carbides, where the M represents a metallic constituent, usually Ti or Nb. All etched bolts exhibited a banded microstructure with the bands oriented parallel to the bolt axis; this is consistent with the reported hot rolling for the bolt material. Examination of the etched microstructures using DIC lighting revealed that the banding was due to regions of carbides aligned in the rolling direction (Figure 6-5). The carbides were mostly intragranular; very few intergranular carbides were present. The microstructure consisted of fine, equiaxed grains (ASTM N°7-8) with occasional very large grains (ASTM N°1-2).

7 Piping, pumps and valves

7.1 Destructive examination

The RV internals at the ONS-1 are comprised of two major subassemblies: the plenum and the core support assembly. The core support assembly is divided into three major subassemblies: the CSS, the core barrel assembly, and the lower internals assembly. Eight vent valve assemblies are installed in the core support shield at ONS-1; Figure 7-1 depicts the typical view of the assembly looking from the interior of the CSS.

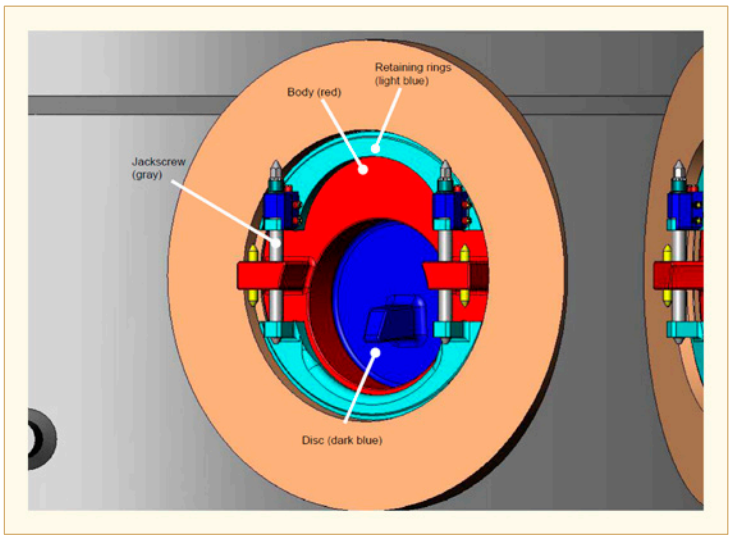

Figure 7-1: Typical B&W core support shield vent valve as seen from the interior of the core support shield.

Each valve assembly consists of a hinged disc, valve body with sealing surfaces, a split-retaining ring and fasteners, and an alignment device to maintain the correct orientation of the valve for operation. The retaining rings are expanded into the core support shield by two jackscrews per vent valve. The jackscrews are torqued and then a locking device is used. In October 2012, ONS-1 shutdown for refueling and completion of various examinations of the RV internals. During that outage, a routine visual (video) examination of the RV internals CSS vent valves was performed. The video examination revealed several abnormal conditions on one of the eight CSS vent valves, although only one will be primarily discussed herein. As viewed from the interior of the CSS, the left jackscrew was extended visibly more than the right jackscrew, causing the lower retaining ring to be rotated slightly and a circumferential crack was identified below the central body boss on the right jackscrew (see Figure 7-2). Review of earlier video inspections showed that the uneven jackscrew extension existed at least a decade prior to this 2012 examination. Additionally, several years earlier, there were indications of bypass flow (visible thermals) with the vent valve closed. However, resolution in these earlier video records was not sufficient to confirm or refute the presence of a crack in the right jackscrew. Video review of the other seven reactor vessel vent valves at ONS-1 showed equal extension of the jackscrews. After entrance into the unit's corrective action program and appropriate actions taken, the apparent cause of the vent valve damage was determined to be impact of the plenum with the top of the left jackscrew during plenum installation, which can occur if the plenum is not level during insertion. The impact forced the lower portion of the left jackscrew through the threads of the lower retaining ring (see Figure 7-2), placing a bending stress on the right jackscrew. It could not be determined whether the right jackscrew cracked immediately from the impact or as a result of increased stresses acting over time. EDM machining was used to separate the jackscrew to allow the entire vent valve assembly to be removed. The vent valve assembly was replaced, and the cracked portion of the right jackscrew was subsequently submitted to failure mode determination [Fyfitch et al, 2014]. The jackscrew material was manufactured from Alloy A-286.

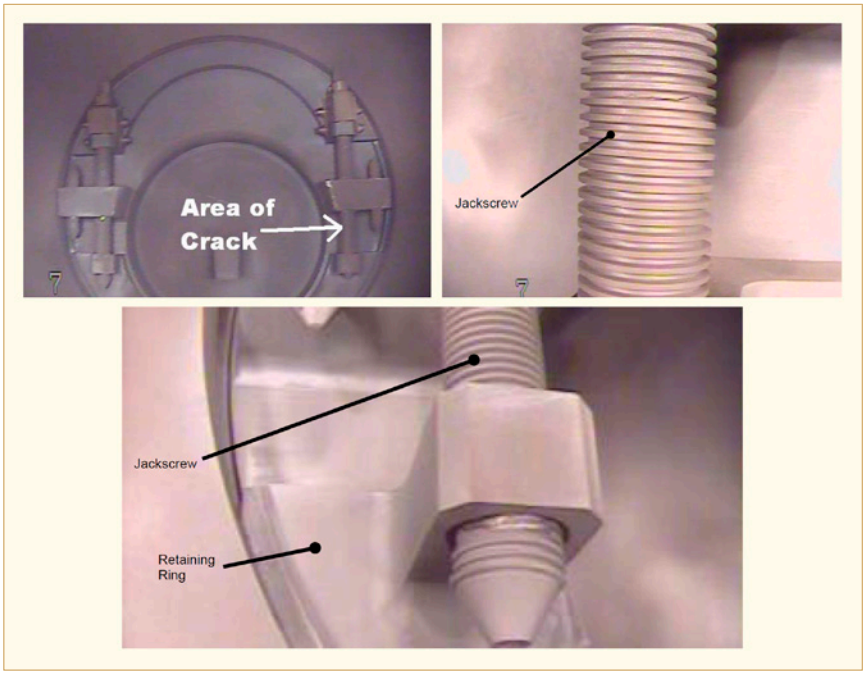

Figure 7-2: Visual examination video capture of ONS-1 CSS vent valve and detail of jackscrews prior to removal. Top left: overview. Top right: right (as viewed from inside of CSS) jackscrew. Bottom: left (as viewed from inside of CSS) jackscrew.

Three jackscrew remnants were received at the lab, including two short sections bounded by the mating fractures and EDM cuts on the opposite ends. The jackscrew remnants were covered with a dark, black oxide (see Figure 7-3 left). The fracture profile exhibited a blocky, brittle appearance and generally followed the root of the thread form with the exception of one location where the fracture ran across a thread crest (see Figure 7-3 left). The mating fracture surfaces were largely covered with a similar dark, black oxide, although a very small crescent-shaped final fracture zone with a fresh, ductile appearance was observed on one side of the screw (see Figure 7-3 right). Ratchet lines and faint arced crack front markings were visible, which were consistent with the crack having initiated on the side of the screw opposed to the final fracture zone (see Figure 7-3 right). Additionally, the origin-side of the fracture surface was stained slightly darker than the side containing the final fracture.

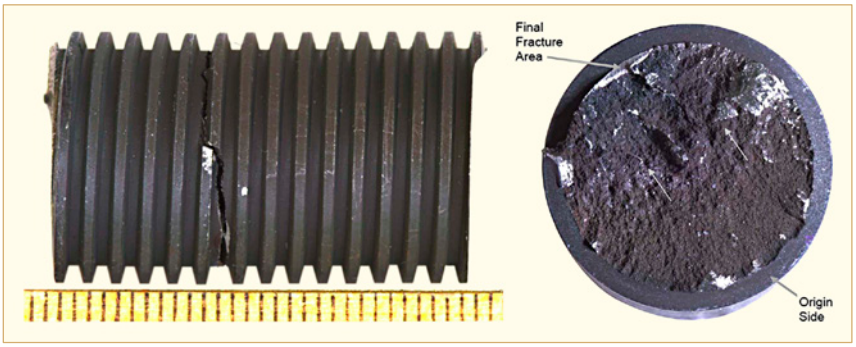

Figure 7-3: Cracked ONS-1 CSS vent valve jackscrew, as-Received. Left: 90° orientation. Right: overview of one mating surface.

A longitudinal metallographic section was taken through the fracture at the origin (see Figure 7-4); review of this metallographic section confirmed that the crack mode was intergranular (see Figure 7-4). Some secondary branching was observed and these cracks were also confirmed to be entirely intergranular (see Figure 7-4). The grain boundaries were decorated with carbides, although there was evidence of an intragranular carbide network as well, possibly from incomplete dissolution of carbides that had outlined the grain structure existing prior to solution treatment. The grain size was relatively fine (estimated to be about ASTM No. 7) and axial deformation bands, suggestive of small amounts of residual cold work, were observed across the jackscrew diameter.

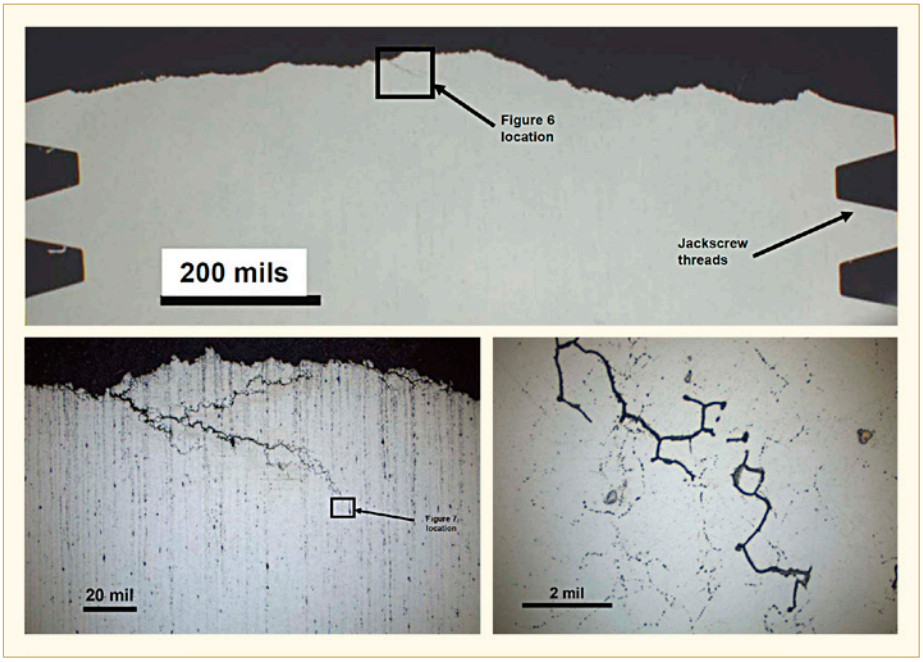

Figure 7-4: Cracked ONS-1 vent valve jackscrew; longitudinal metallographic section taken through jackscrew showing closer view of intergranular branching (oxalic acid etch).

In summary, the failure mode for the ONS-1 CSS vent valve jackscrew was IGSCC. The fracture characteristics were consistent with the presumed failure scenario (i.e., a bending stress was applied to the right jackscrew due to impact loading and failure of the threaded connection on the left jackscrew). Heavy, dark, black deposits present on the fracture surfaces indicate the crack was probably present for more than one operating cycle. The small, final fracture zone indicates the jackscrew did not completely sever in service, but likely separated during the removal process. The composition, microstructure and hardness of the jackscrew was consistent with Alloy A-286 material having a small amount of cold-work with a low-temperature solution treatment (e.g., 890°C) followed by age-hardening. No chlorides or other specific contaminants were identified that would have contributed to the jackscrew failure.

There have been past failures of A-286 components exposed to LWR environments, with the failures being mainly attributed to IGSCC resulting from high stress levels, that is, on the order of the material yield strength or higher. For example, B&W reactor internals bolts were fabricated from ASTM A-453, Grade 660, Class A/B materials. IGSCC failures were detected in several plants in the early 1980s after only a few years of operation. Typically, failures only occurred in cases where the calculated stresses exceeded yield stress, and failure rates increased with increasing stress levels. There has been some limited evidence (e.g., transgranular crack propagation), suggestive of fatigue assisted crack initiation; however, there was no evidence of transgranular crack propagation in the ONS-1 CSS reactor vent valve jackscrew.

8 Steam generator

8.1 Operating experience

About 60 PWRs worldwide are operating with SG tubes made of alloy 600TT, among which 27 are located in France. This alloy is susceptible to corrosion, both on the primary and secondary side in every fleet, though with different time scale or extent. The reference [de Curières et al, 2014] gives an overview of the international operating experience of this alloy and indicates the associated controllability and safety-related issues. An emphasis is put on the manufacturing, chemistry and specificities of the different fleets. The French situation is reviewed in this frame. It is noteworthy that many of the primary side corrosion issues can clearly be explained by design or operating conditions. However, destructive examinations show that all the secondary side issues are much hardly explained by simple considerations, even though they prove challenging for the safety of plants.

It has been shown previously that the PWSCC affecting the various fleets can be widely explained by the following various factors:

- The type of rolling/expansion, which explains the various initiation and propagation kinetics and also the orientation of the cracks, even for those occurring in the tubesheet at tube ends in the tack roll/expansion transition;
- The presence of hard sludge/deposits, or denting, on the secondary side, which explains circumferential cracks on the ID of the tubes;
- Applying shot-peening to already operating steam generators, which does not compulsorily suppress the initiation of cracks, initiation being defined here as the detection threshold by NDE techniques. This may be ascribed to the fact that this mitigation technique has been applied when cracks were already initiated, but still below the threshold for NDE detection. However, shot peening applied before operation seems to suppress PWSCC.

Since 1990, a few plants are suffering from IGA/ODSCC (about 10 plants affected worldwide), however, the number of affected tubes is growing, though still very small in comparison with the number of tubes affected by PWSCC. Plants are affected in the USA, Korea and France. If ODSCC of alloy 600TT tubes has occurred since 1990, a precursor of ODSCC befell in a French plant in 2012, where multi circumferential cracks were found in the interstice between the tube and the tubesheet, below the last contact point, based on the pulled tube inspection. Worldwide, cracks were detected at the TSP and TTS level, and sometimes in the freespan region. The French precursor remains thus a unique event in the world.

It appears that the susceptibility of alloy 600TT tubes to IGA/ODSCC may be ascribed to a combination of various factors. The reference [de Curières et al, 2014] notes however that:

- A “non optimized” microstructure is not always reported;
- The presence of high residual stresses does not always lead to ODSCC, for example, one US plant has 40 tubes with high residual stresses, and nevertheless no indication of ODSCC in 2011.

From the DEs and NDE, it appears that, if high residual stresses or a “non optimized microstructure” are factors found on some pulled tubes where IGA/ODSCC occurred in the freespan region or at the TSP level, chemistry is the main factor influencing IGA/ODSCC at the TTS location. Indeed, most pulled tubes examinations with IGA/ODSCC have shown the presence of pollutants.

DEs of pulled tubes made of 600MA reveal that the morphology of ODSCC can be very complex with multiple initiation sites and branches. Modeling can be used for the analysis of eddy current probes response to various parameters of flaws. For example, CIVA[2] can be used to evaluate the effect of the orientation of flaws on the amplitude of the signal. The residual constraints in 600TT tubes are lower than for 600MA tubes, so the balance between longitudinal and circumferential OD stresses might be different. It is therefore useful to evaluate the probe response for flaws which could deviate from a perfectly longitudinal or circumferential crack. For this application, the CIVA model chosen is planar (simplified approach). Several rectangular notches with a length of 6 mm, a width of 0.1 mm and a depth of 40% TW are considered. The notches are located at the outer surface of the slab. Their orientation varies from 0° to 45° (see Figure 8-1 top left). The response of different probes are given in Figure 8-1 top right for a Transmit/Receive probe in differential mode, in Figure 8-1 bottom left for a differential probe and in Figure 8-1 bottom right for the +Point. A slight drop of -2 dB in amplitude can be observed between the reference notch and the notches with a skew up to 20°. This drop is small with respect to the overall reproducibility of the techniques used for in service inspection. For a very large skew of 45°, a significant attenuation is observed for the +Point probe due to its technology based on cross-wounded coils. This phenomenon is well known and can be addressed using a combined +Point probe and pancake probe. This example shows that parametric studies can be performed with an industrial simulation tools and can be used to evaluate probe performances.

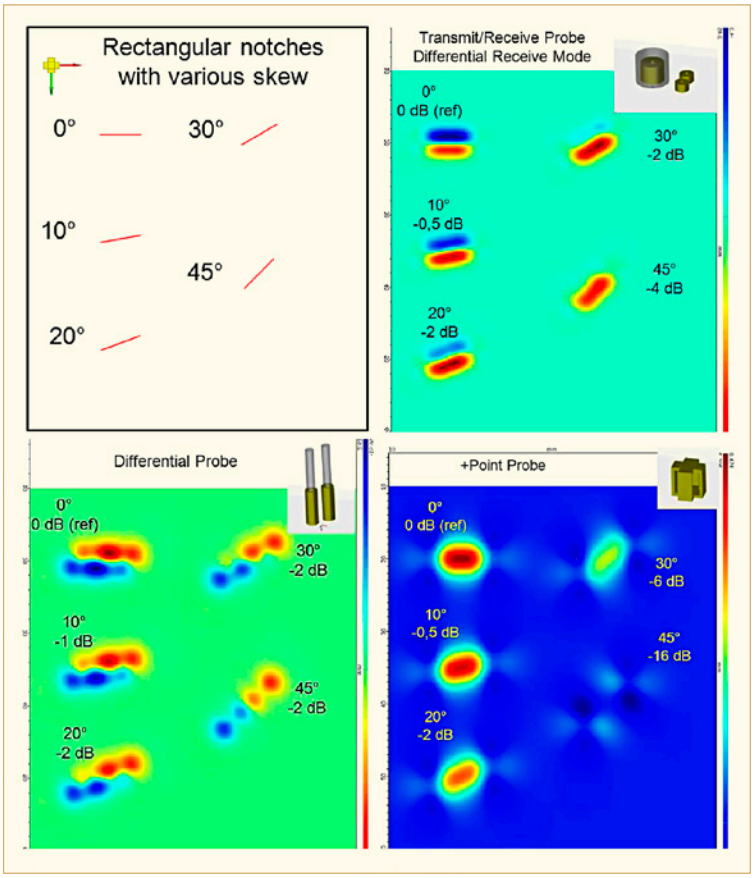

Figure 8-1: Top left: geometry for the analysis of eddy current probe response with respect to the orientation of a rectangular 6 mm notch, 40% TW, located at the outer surface. Top right: response of a Transmit/Receive probe in differential mode. Bottom left: response of a differential probe. Bottom right: response of the +Point probe.

[2] CIVA is a computer code dedicated to the modeling of nondestructive testing techniques (UT, RT, ET). It is developed by the CEA.

Considering that IGA/ODSCC defects are an issue with respect to the safety of the plant, namely the integrity of one of the containment barrier, and that they may happen in properly manufactured tubes, it is important to adapt the inspection program to actual and foreseen degradations. Innovative technologies such as ET array probes can improve the detection of the early stages of ODSCC for the entire length of Alloy 600TT tubes and could be implemented more by the industry.

Almaraz Units 1 and 2 operate three Siemens W-61 replacement SGs. The tubing material is TT Incoloy 800. The design dimension of all tubing: 19.05 mm OD and 1.09 mm nominal wall thickness. The tubesheet is 615.7 mm thick. The tubes have a full depth hydraulic expansion with an additional hard roll at the tube-end and just below the top-of-tubesheet. Almaraz SGs were replaced in 1996 (Unit 1) and 1997 (Unit 2). In 2006 denting was detected in the SG-3 of Unit 2 and in subsequent years the denting was increasing in the tree SG's of the two units. During the 2R19 outage held in May 2009 at Unit 2, ten tubes were examined for circumferential indications, reported by ET, and all exhibited circumferential OD indications with the UT technique. Circumferential indications were detected in the transition zone of the tubes near from tube-sheet.

Tubes with denting are associated with hard sludge, but some tubes presented denting with soft sludge. The number of tubes affected by denting is higher in the cold leg than in the hot one, while circumferential indications are observed at the opposite legs.

MRS replacement in 2007 and 2008, unit 2 and unit 1 respectively, produced an increase in the impurities input. Besides, a resin input occured in the three SG's of Unit 2 in 1996. Crevice chemistry estimation, between the tubesheet and the tube, indicates a neutral or slightly caustic environment. However, the latest study conducted in 2009 indicated a trend towards lower pH in the GV3 of Unit 2.

During outage held in November 2010 at Unit 2, three tubes of the SG-3 were pulled out for DE. Two of them were sent to Areva´s laboratory and the third (R67C48) to CIEMAT.

The reference [de Diego et al, 2014] presents the results of the DE of R67C48 SG-3 tube from Almaraz unit 2. This tube had circumferential ET indications in the expanded transition zone and denting with 46 mm height of sludge. Figure 8-2 shows the as-received R67C48 230 mm segment tube. Three areas were marked on the tube surface: free tube, transition zone and expanded zone. Zero is also marked for recording observations collected along the tube perimeter.

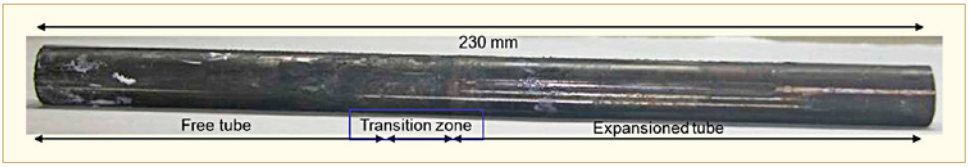

Figure 8-2: As-reception segment tube R67C48, SG3- Almaraz 2.

Figure 8-3 shows the existence of an area 5 mm wide with multiple circumferential small cracks, separated by ductile ligaments. These cracks are located at 3 mm from last contact point between the tube and the tubesheet. Damage as "wastage", pitting or other has not been detected.

9 Steam-water system

9.1 Operating experience

The main function of the Steam Generator Blowdown System is to purify the secondary water from all kinds of pollutions: corrosion products from the secondary system, consequences of raw water pollutions through condenser's leakage, potential radiochemical pollutions resulting from Primary-to-Secondary leaks.

Purification of the secondary water is performed by:

- Filters to eliminate all non-soluble species;
- Ion exchange resins to remove the soluble species.

Nevertheless, the use of resins, mainly made of polymers, implies cooling down the secondary water below 60°C before passing through the resins. This is possible thanks to SGBS heat exchangers.

The performances of the purification system are also directly correlated to the availability of the SGBS heat exchangers. In case of degradation of the exchanger, to avoid any degradation of the resins due to high temperatures, the purification system is by-passed and the pollutants of the water are not removed anymore. Such by-pass may have consequences on the integrity of the secondary circuit's components since corrosive pollutions are not eliminated (halides or sodium) and corrosion products could contribute to SG fouling and TSPs blockage. Through these potential impacts, the effectiveness of the SGBS heat exchangers is so indirectly linked to the nuclear safety of the nuclear power plants and more directly to their performances.

To ensure the maintain of the safety and performances levels of its plants, EDF has reviewed its operational experience about the SGBS to identify the main observed malfunctions and define the corrective actions to initiate.

The topic of the reference [Praud et al, 2014] is to present the main SGBS dysfunctions linked to the degradation of the tubular heat exchangers, which sometimes can lead to integrity failure, through corrosion phenomenon.

Three kinds of degradation can happen to the SGBS heat exchangers:

- Mechanical degradation due to fretting of tubes on the various kinds of plates;
- Thermal and mechanical fatigue;
- Internal and external corrosion of tubes' surfaces.

Fretting and fatigue are mainly linked to the design of the heat exchangers. Few mitigation means are available in operation against these kinds of degradations. Moreover, neither fretting, nor fatigue has been observed as root cause of degradation on EDF fleet. That is why we will focus on the corrosion degradation. In the following chapter, the different mitigation techniques will be developed.

Non-regenerative heat exchangers. For the non-regenerative heat exchangers, where the tubes OD is in contact with the CCS conditioning chemical (Na_3PO_4), caustic corrosion can occur. This corrosion is observed at the TS or at the TSPs flow holes where Na_3PO_4 can hideout and be decomposed into caustic ($2Na_3PO_4 + 3Ca(HCO_3)_2 \rightarrow 6NaOH + 6CO_2 + Ca_3(PO4)_2$).

Historically, this degradation has been observed on the oldest 3-loops plants, which were equipped with SS tubes. SS tubes being prone to caustic corrosion (Figure 9-1), these tubes have been replaced with LAS tubes which are less susceptible. Also, full depth rolling has been implemented on new exchangers. However, LAS tubes can also suffer from caustic corrosion (Figure 9-2) in the hottest areas of the bundle (close to the hot channel head).

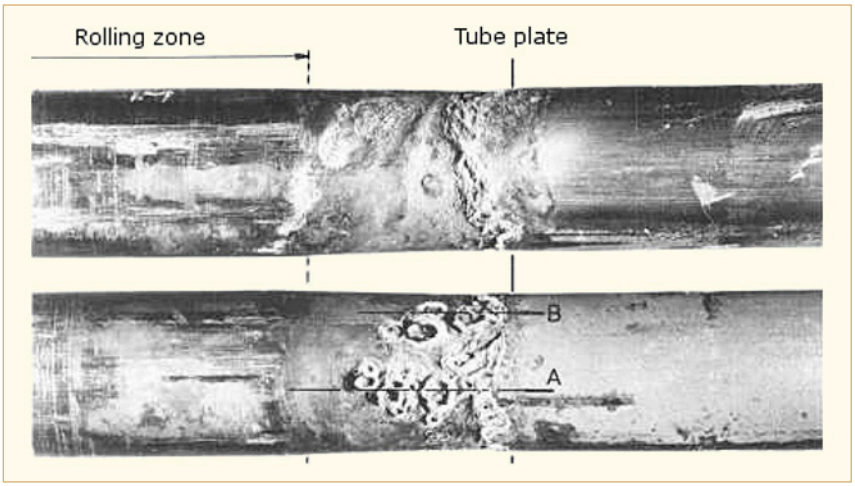

Figure 9-1: View of a SS tube suffering from OD caustic corrosion (1986). Non-regenerative heat exchanger of a 3-loop unit.

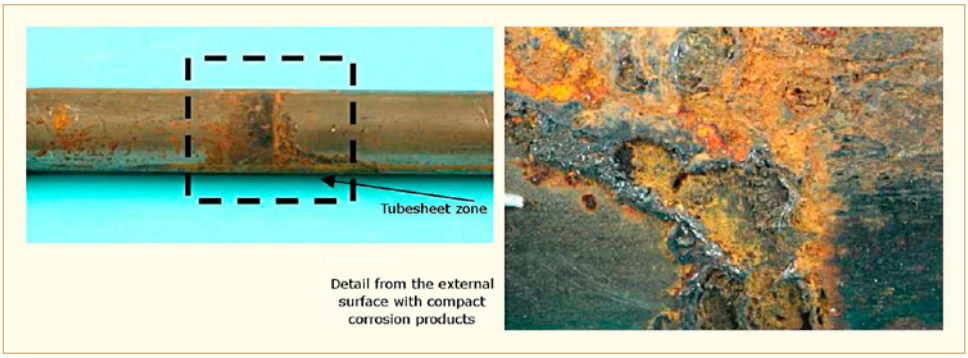

Figure 9-2: View of a LAS tube suffering from OD caustic corrosion (2006). Non-regenerative heat exchanger of a 3-loop unit.

Regarding the tubes ID of non-regenerative exchangers, no TW defect has been observed so far. However, visual and destructive examinations have shown that the degradations observed on the regenerative exchangers can occur on the non-regenerative ones, without reaching TW.

As concerns mitigation, as mentioned previously, the material and the rolling process have been modified. Despite this, the caustic corrosion is still active.

Regenerative heat exchangers. In these exchangers both sides of the tubes are in contact with the secondary water, only the temperature is different.

The tubes ID can experience pitting and under deposits corrosion or differential aeration corrosion (Figure 9-3). Indirect attack can also occur because of the fluid turbulence associated with the flow over and around the deposits or resulting crevice. This kind of corrosion is always located around the bottom of the tubes and associated with an inappropriate layup. As shown on Figure 9-4, the corrosion is ID initiated and can be TW.

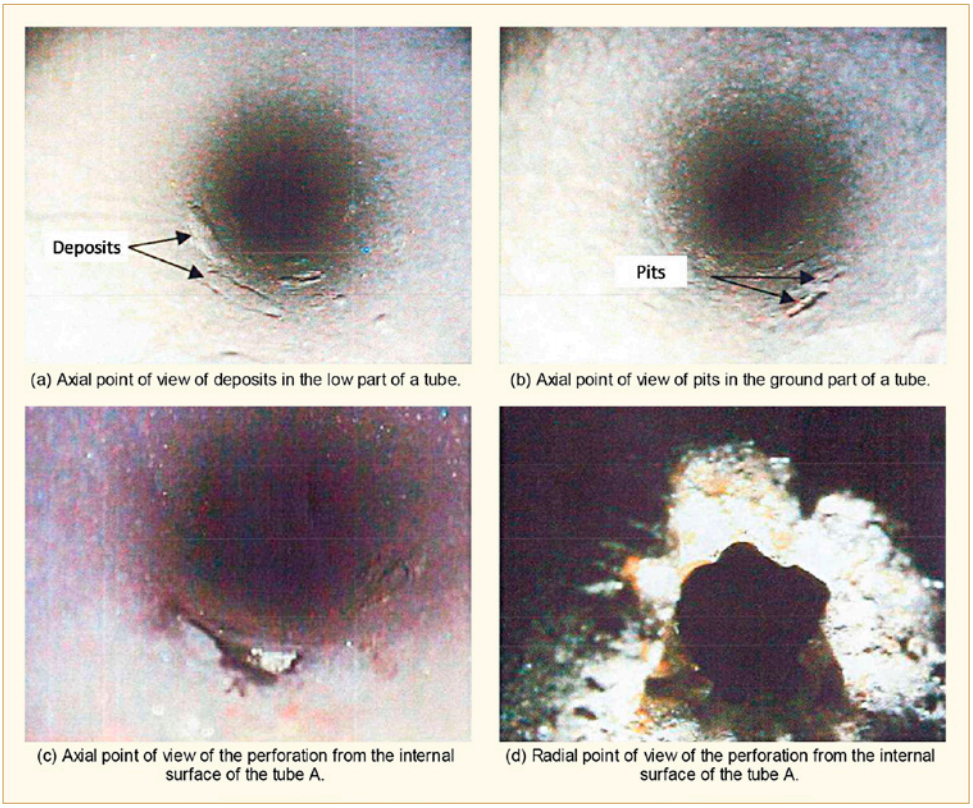

Figure 9-3: View of the ID of tubes from a regenerative heat exchanger of a 4-loop unit. Pictures from outage VT.

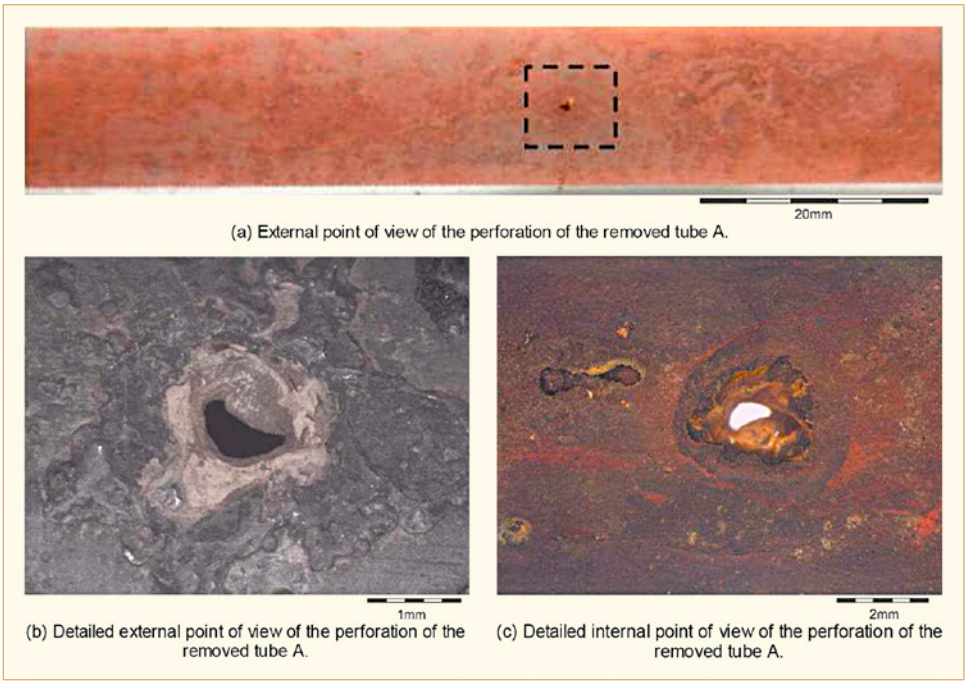

Figure 9-4: Views of a leaking tube from a regenerative heat exchanger of a 4-loop unit. Pictures from outage VT.

A tube leak may induce FAC (Figure 9-5) or erosion of adjacent tubes, sometimes leading to tubes ruptures (Figure 9-6).

10 Turbine, main generator (alternator)

10.1 Operating experience

Even if nuclear steam turbines are commonly designed considering identical blades, there are always some random deviations among the blades due to the manufacturing tolerances, wear, erosion… leading to a small natural mistuning between the blades (e.g. natural frequency shift of the blade of about 1%). Mistuning may lead to harmful impacts on the blade vibrations, the stresses and the mechanical strength regarding the high cycle fatigue [Roques et al, 2014].

The LP steam turbines of the 900 MW CP2-1300 MW units are reaction-type with welded rotor technology (80 double-flow rotors). Amongst the 10 stages per flow, the last stage has 77 free-standing blades per row, with a curvilinear fir-tree root (see Figure 10-1).

Figure 10-1: Overview of LP turbines of EDF CP2-1300 MW units.

Based on the feedback of non-EDF nuclear steam turbines, nondestructive testing was added to the maintenance program since 1996: over the 12,320 LSB of the fleet, only 5 cracked blades were found. Cracks were located at the notch #1; one blade had also an atypical crack on the notch #2 (Figure 10-2).

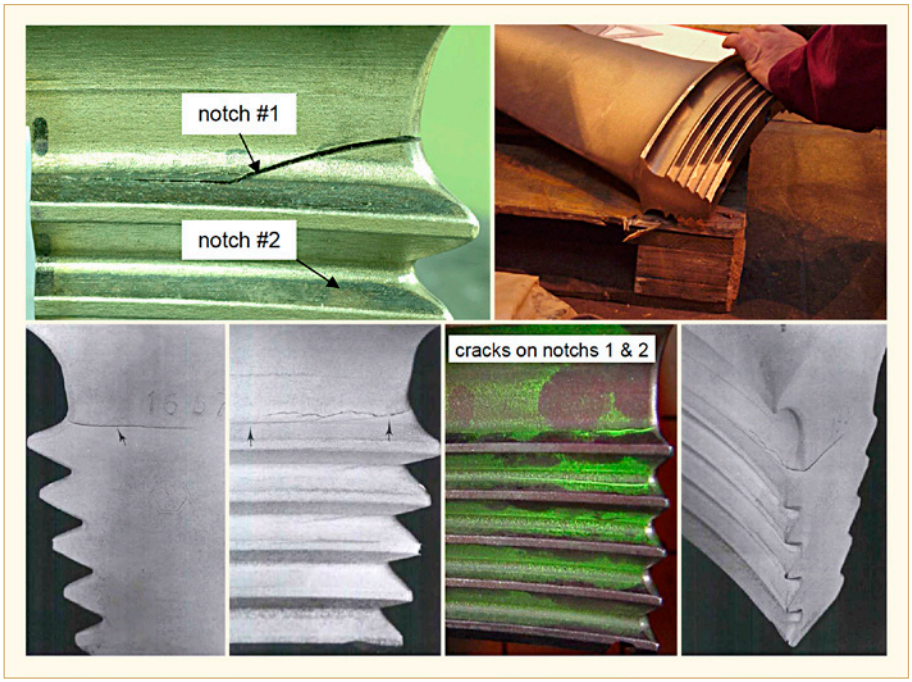

Figure 10-2: Example of cracking of last LP stage blade.

To prevent the growth of cracks, one solution consists in reducing the level of vibrations. This can be achieved either by optimizing the natural mistuning of the blades but requires initial data such as the original blades and previous blades vibrations measurements (not available), or by imposing a forced mistuning which appears to be a better industrial solution. EDF decided to do an experiment on one LP module by permuting 4 specific blades in order to reduce the highest blade vibration level (i.e. blade #14, see Figure 10-3). As shown in Figure 10-4, this experiment gave satisfactory results with a significant reduction of the blades vibration.

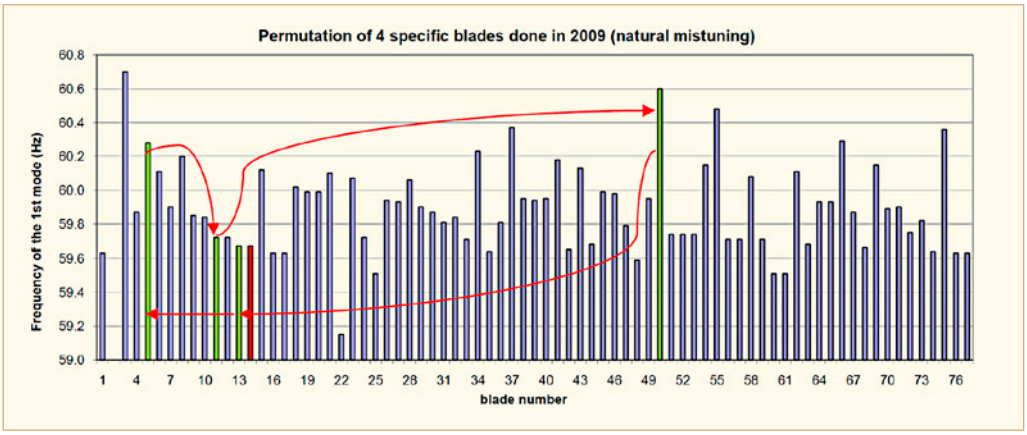

Figure 10-3: Blades eigenfrequencies of the 1st mode and principle of permutation.

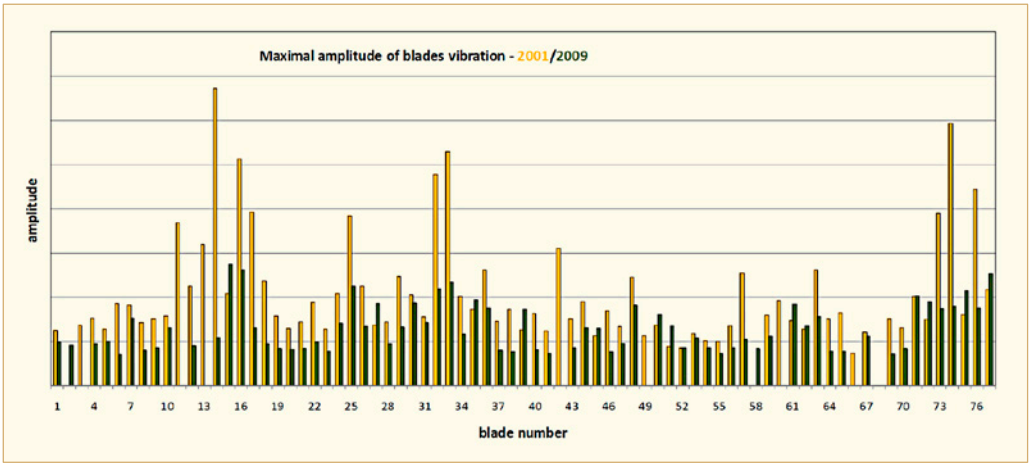

Figure 10-4: Comparison of the level of vibrations of the blades before and after the permutation.

The Figure 10-5 shows how beneficial the blades permutation was regarding the vibration level of the blade #14.

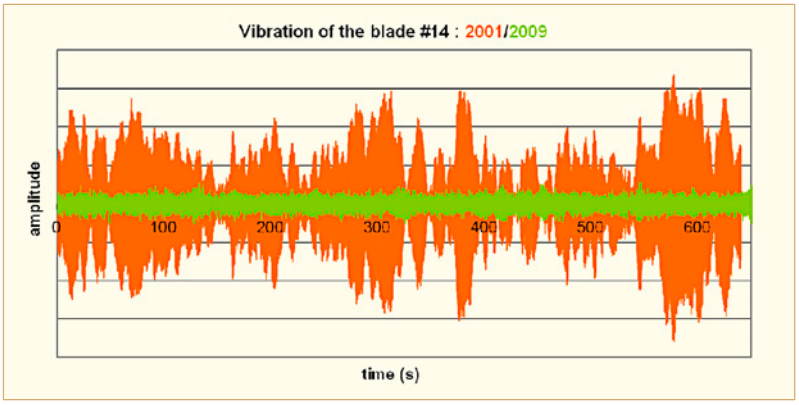

Figure 10-5: Comparison of the vibration of the blade #14 before and after optimizing the natural mistuning.

The technical feasibility is now acquired and the implementation study of the mistuned bladed assembly on site on a LP1 module with a BVM system is validated. The final decision to implement such modification is pending on the profitability study (currently in progress).

Some of the CP1 1,000 MWe Nuclear Steam Turbines have already been successfully retrofitted worldwide. The implementation of this proven solution in the Koeberg NPP has been applied in addition with new technical features in the steam path; new blading technology associated to steam balance holes, drilled in the rotor disk of the stages 2, 3 and 4, provide a higher performance improvement. This modification led to difficulties during commissioning of the Unit 1 in October 2010. Following initial ramp-up to full speed, overspeed test and synchronization, the unit was loaded to 240 MWe before tripping due to high vibration on LP1 rear bearing. A root cause analysis was performed to determine the origin of the problem characterized by radial rubbing and diaphragm bolts stretching. Jointly with ESKOM, ALSTOM took immediate interim actions to allow the return to service without vibration incidents and the unit reached full load in December 2010. Alstom has subsequently carried out a root cause analysis of the vibration incidents and has established that a temperature difference between the inner and outer rings of the diaphragms was at the origin of the problem. Finite element calculations simulating this temperature difference have been carried out to assess the mechanical integrity of the diaphragms and design changes have been proposed for safe and reliable long term operation of the two units. The reference [Buguin et al, 2014] describes the results of the investigation and root cause analysis and the proposed design changes for the two units at Koeberg.

Following the erection of the new components in October 2010, the first commissioning tests were performed successfully. The initial run up to 1,500 rpm was without incident. After overspeed and synchronizing checks, the unit was loaded up to 240 MWe on the 1st of November 2010. The unit was manually tripped due to LP1 rear vibration reaching 180 µm p-p. Two further runs were carried out on the 2nd and 3rd of November 2010, with similar outcome. The machine was stopped and additional investigations launched to determine the causes of the vibration. Visual and dimensional inspections showed that rubbing had occurred at the hub in the bottom half at stages 3 & 4 in all 3 LP cylinders with the worst in LP1 (Figure 10-6 left). Evidence of light rubbing was also visible on stages 5 & 6. The rubbing in LP3 was very light. No top half radial rubbing was seen. Most of the diaphragm bolts on stages 3 & 4 and 5 & 6 were found loose and numerous bolts were found stretched.

A simple 3D FE calculation was done on a typical diaphragm with the thermal field corresponding to representative conditions of a stage 4 to investigate the displacements caused by thermal effects. The thermal conditions taken into account for the initial mechanical calculations were based on a theoretical throughflow calculation at design operating conditions. These assumptions were confirmed by temperature measurements installed on diaphragm rings (Figure 10-6 right). The implementation of steam balance holes increased the temperature of the diaphragms inner rings. It is due to the throttling of the superheated leakage of the stage 2 towards stage 5 through the balancing holes.

11 Fuel, control rod assembly

11.1 Fuel failure and operating experience

To protect man and environment against artificial radioactivity, 3 barriers have been erected in the NPPs. The first barrier, the cladding and end plugs of the fuel rods, confines the fission products in the fuel rods free volumes and pellets. Does a leak tight first barrier mean no fission products in the primary circuit coolant? No, as a small quantity of fissile uranium is always present in the coolant: some pellet dust coming from the fuel manufacturing plant and unavoidable trace impurities of uranium in zirconium alloy cladding. Monitoring of the fission product activities during the reactor operation cycles is necessary to detect any failures of the first barrier. A leaking rod can release fission gases, volatile fission products (Iodine and Cesium) and pellet fissile material. This can lead to big issues such as longer outage periods, unanticipated shutdown, potential increased doses for the workers and higher radioactivity release outside the reactor or in the waste. The first glimpse we have on these potential issues is only coming from the coolant fission product gamma activities. For a long time, radiochemistry assessments have been, intensively worked on and expanded by AREVA and other entities. These classical assessments are presented in the reference [Petit et al, 2014].

Nuclear industries developed an intolerance towards fuel failures and a “way of working” to minimize the fuel leakage issues. These efforts resulted in significant reduction of number of failed assemblies in recent years. Nowadays, most nuclear cycles are leaker free, some have one failed rod, more seldom several failed rods. At the same time, most operating radiochemistry limits for the coolant and for external releases have been reduced.

This improvement of fuel reliability rendered more and more visible a previous “no issue” phenomenon: fuel leakages releasing very few fission products during the cycle and hard to detect during the outage. These “weak leaks” bring problems as will be reported and developed in this paper. The weak leaks shake the foundations of radiochemistry assessments and challenge the sipping test and examination devices. During the cycles, the activity limits will not be reached but the outage may be longer as more time may be needed to identify the failed assemblies.

In PWR, the FP activity in coolant reaches equilibrium between release (birth) and disappearance (death). Release depends upon fission rate inside the tramp uranium and the failed rod. Disappearance is due to radioactive decay and purification rate. At stable reactor conditions (power, purification rate) this equilibrium leads to stable FP activity level. At such conditions quick changes of this level can only increase and are due to the occurrence of other leakages in the existing failed rod (secondary defect) or among the other rods (additional failed rods). Some slow changes in activity level will occur, including decreases, when the failed rod power changes. These kinds of slow changes will take place during the whole length of a cycle. This “medium or usual or classical” behavior is observed with high, medium or low FP activity levels: see Figure 11-1. Low activity levels take place in case of low tramp U activity and the presence of only one failed rod with a low power, for instance a gadolinium rod during its first cycle. In the real radiochemistry life, more and more cycles do not follow the above description. These “non classical” cycles exhibit strange behavior such as no Iodine spike during shutdown transient, no FP release during a few months, release of Xenon 133 alone with “roller coaster “ (strong up and down) in activity levels. See Figure 11-2 as an example. For other cycles, the date of opening of the leak was misevaluated, as the period of no fission product release was not acknowledged. See Figure 11-3. These defects releasing very few fission products were sometimes masked, e.g. by another usual leakage, or by a high tramp uranium background level. The definition of the a weak leak cycle is the following: a weak leak cycle is a cycle having, after the opening of its fuel defect, a release of Xenon 133 solely during at least two weeks or having a period of no FP release from the defect.

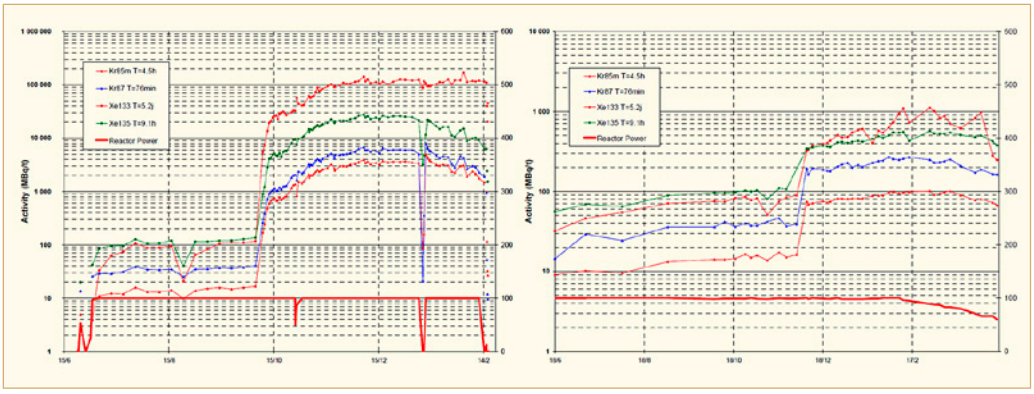

Figure 11-1: Medium leak cycle. Left: with high power failed rod (300 W/cm). Right: with low power failed rod (89 W/cm).

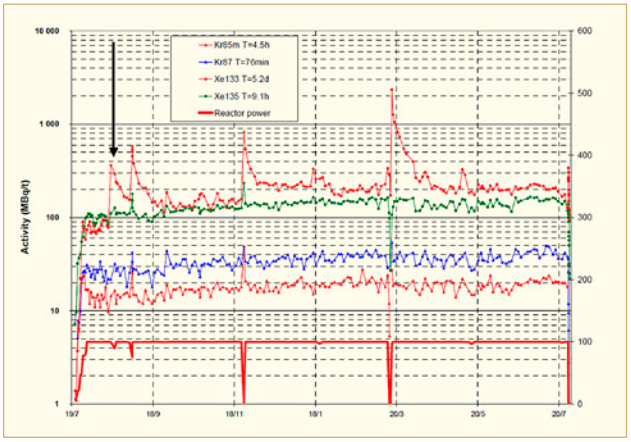

Figure 11-2: Weak leak cycle: no Increase of Xenon 135 and spikes of Xenon 133.

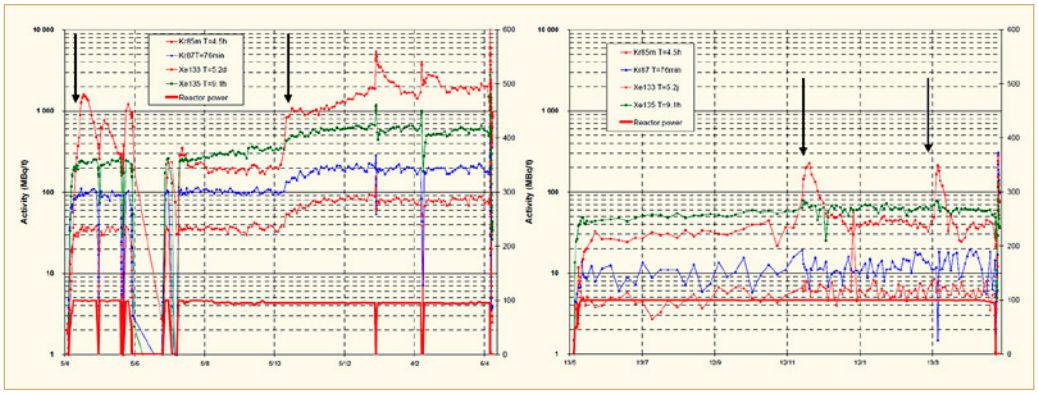

Figure 11-3: Left: weak leak cycle then medium leak cycle due to the opening of a secondary defect. Right: weak cycle with only two short periods of Xenon 133 release.

This new oxide layer is of no importance for a big primary defect of a size equal to 1 or more millimeters. In case of tiny primary defect, this oxide layer can have a noticeable effect. For instance, a 0.44 µm crack will be sealed by oxidation in a one month period. A smaller passageway of 0.014 µm, 70 times the size of an atom, will be sealed in one day. Weak leak cycles often have an unstable activity level of Xenon 133. As it takes a long time to pass through the fuel defect, the Xenon 133 activity level is not a function of the failed rod power but is a function of the size of the defect. Any change in the defect size will affect this level. During power transient, thermal expansion induces a temporary change in stress in the cladding surrounding the defect and a change in the defect size results in a notable release spike of Xenon 133. With time, oxidation of the defect lips can provoke a decrease in Xenon 133 activity and can even lead to a stop in fission product release from the defect. Conversely, an enlargement of the defect size (due to any reason) allows more Xenon 133 and possibly also short life fission gases to escape. If there is enough water inside the failed rod, a secondary defect can open and the failed rod will release "as usual" all fission products. In the past, Xenon 133 activity was a function of rod power mainly, while the size of the primary defect was a secondary parameter. For weak leaks, this relationship changes to its opposite, the size of the primary defect becomes larger and Xenon 133 activity does not depend on a rod power.

In presence of a weak leak cycle, the radiochemist analyst needs to be very cautious and follow the following rules and guidance:

- The occurrence of a first weak leak is easy to spot in case of low Tramp U level: an increase of Xenon 133 alone and above the Xenon 135 activity level. In case of high Tramp U level, all the increases in Xenon 133 activity must be considered and compared with the past activity levels (of the BOC or of previous cycle levels) and with the other gas activities. The Xenon133 / Xenon 135 ratio could stay below 1 even in case of a fuel defect;
- Failed rod power estimation cannot be performed;
- MOX – UO_2 discrimination (based on the ratio Xenon 135 / Krypton 85m) cannot be performed;
- Estimation of the number of cycles of the failed assembly (based on the release of Cesium during power transient) cannot be performed.

During this first stage, the only possible estimation is the presence of one failed rod with a weak leakage. As time passes by, fission product activities may increase with the failed rod releasing more fission products, and the classical assessment methods may become useable. This activity increase can be due to:

- The widening of the primary defect;
- The occurrence of secondary defects;
- The occurrence of a second weak leak failed rod;
- The occurrence of a second medium failed rod.

The distinction between these four scenarios is not easy to draw. In case of an increase of Iodine, the most probable explanation is the occurrence of secondary defects.

If a weak leak occurs after a medium failed rod, the second failure is impossible to identify as long as it has a weak release and "one train can hide another" warning is also valid for failed fuel analysis. Estimation of the number of failed rods is based on the FP activity level and also uses a probabilistic approach. A fuel reliability engineer analyzing a fuel failure can obtain additional insight on the nature of the failure and an estimate of a number of failed rods using the previous reliability experience feedback from the same fuel, which may also include previous manufacturing issues at fuel fabrication facility.